Performance Analysis for Supporting Ultra-Reliable Low-Latency Communications in Advanced Wireless Networks

by

Nhat Hieu Le

A thesis submitted to the Faculty of Graduate and Postdoctoral Affairs in partial fulfillment of the requirements for the degree of

Master of Applied Science

in

Electrical and Computer Engineering

Carleton University
Ottawa, Ontario

Abstract

A new approach that combines physical and link layers is introduced to estimate the performance of wireless systems that support ultra-reliable low-latency communications (URLLC). Motivated by ultra-dense network setups in advanced wireless systems to achieve high-peak data rate and high reliable connectivity, the effects of spatial diversity of multiple base stations are investigated with analytical expressions for evaluating signal-to-noise-and-interference-ratio (SINR) coverage probability at the physical layer and the average blocking probability at the link layer. The impact of network densification on the average blocking probability, which is of practical interest to network carriers, is studied with numerical results. Specifically, it is shown that considering the second nearest station to exploit the spatial diversity of multiple base stations offers an order of magnitude improvement in the average blocking probability. Numerical results also show that SINR coverage and average blocking probabilities achieve optimal values at different cell sizes for either a single nearest station only or two closest stations. The proposed approach can be generalized to utilizing more than two base stations through a recursive process. Our approach can help providers optimize their network performances for supporting URLLC services while saving their costs.

Acknowledgements

First and foremost, I would like to thank my supervisor, Professor Changcheng Huang, for his patient and outstanding guidance during this research. His helpful feedback and constant encouragement have made this thesis possible. I feel fortunate to work with Professor Changcheng Huang. I am always grateful for all the support from my dear family (my parents, siblings, and lovely wife). Without them, I could not carry on this journey all by myself in Canada. Moreover, I want to express my gratitude to my friends (Uyen and Khai) who help me proofreading. Lastly, I would like to thank all my teachers at Carleton for conveying valuable knowledge to me.

Table of Contents

List of Tables

List of Figures

List of Acronyms

3GPP	The Third Generation Partnership Project
5G	The Fifth-Generation mobile network
5G-NR	The fifth Generation New Radio
BS	Base Station
CCDF	Complementary Cumulative Distribution Function
eMBB	Enhanced Mobile Broadband
HARQ	Hybrid Automatic Repeat Request
LoS	Line-of-Sight
mmWave	Millimeter-Wave
mMTC	Massive Machine Type Communications
NLoS	Non-Line-of-Sight
OFDMA	Orthogonal Frequency-Division Multiple-Access
PDF	Probability Density Function
PPP	Poisson Point Process
QoS	Quality of Service
SINR	Signal-to-Noise-and-Interference-Ratio
TTI	Transmit Time Interval
UE	User Equipment
URLLC	Ultra-Reliability and Low-Latency

List of Notations

Φ	PPP for outdoor BS locations
λ	Outdoor BS density
$\boldsymbol{X_i}$	Location of i-th BS
Φ_u	PPP for mobile station locations and
λ_u	Mobile station density
$b(r)$	LoS probability function that the link with length r is LoS
$\boldsymbol{R_0}$	Random variable of the link length from a typical user to the serving BS
$\boldsymbol{R_i}$	Random variable denoting the distance from a typical user to i-th interference BS.
$l(r)$	Path loss function at a distance r, where $r > 0$
C_p	Intercepts of path loss formulas for LoS and NLoS links, where $p \in \{L, N\}$
α_p	Exponents of path loss formulas for LoS and NLoS links, where $p \in \{L, N\}$
M_i	Main lobe directivity gain at either a transmitter or receiver, where $i \in \{T, R\}$
S_i	Back lobe gain at either a transmitter or receiver, where $i \in \{T, R\}$
θ_i	Half-power beamwidth of the main lobe at either a transmitter or receiver, where $i \in \{T, R\}$

G_0	The total directivity gain in the serving link
$\boldsymbol{G_i}$	Random variable denoting the total directivity gain in the link from i-th BS.
A_k	PMF parameters of the random variables $\boldsymbol{G_i}$, where $k \in \{1,2,3,4\}$
B_k	The probability that $\boldsymbol{G_i} = A_k$, where $k \in \{1,2,3,4\}$
$\boldsymbol{H_0}$	The small scale-fading of the serving link
$\boldsymbol{H_i}$	The small scale-fading of the i-th interference link, where $i > 0$
P_t	Transmit power of BSs in Φ
σ^2	Normalized Noise Power by P_t
V	mmWave Carrier Frequency
N_p	Nakagami fading parameter of LoS and NLoS links where $p \in \{L, N\}$
R_λ	Average cell radius corresponding the BS density λ
$\boldsymbol{\gamma_{D,i}}$	Random variable of downlink SINR at the first or the second base station where $i \in \{1,2\}$
$f_p(r)$	PDF of the distance to the first LoS or NLoS station where $p \in \{L, N\}$
$A_p(R_\lambda)$	Association probability of a typical user for $p \in \{L, N\}$ when the average cell radius is R_λ
$\hat{f}_p(r)$	PDF of the distance from the serving station to a typical user for $p \in \{L, N\}$
γ_i	Target SINR threshold at the first or the second base station where $i \in \{1,2\}$

$P_{C,i}(\gamma_i, R_\lambda)$	SINR coverage probability of the first or the second station at SINR γ_i and the average cell radius R_λ; where $i \in \{1,2\}$
$P_{C,1/2}(\gamma_1, \gamma_2, R_\lambda)$	The joint CCDF of the downlink SINR outage probability at the first and second base stations
W	Total available bandwidth
D	QoS requirement for URLLC packet where the packet must be delivered total delay of D seconds
Δ	QoS requirement for URLLC packet loss
M_c	Maximum re-transmissions for a URLLC packet to class c users
$D_{i,c}$	Maximum delay feedback at the first or second station of class c users where $i \in \{1,2\}$
$\bar{\lambda}$	The average number of users within a BS's Voronoi diagram
$\hat{P}_i(c; R_\lambda)$	Probability that users are classified into class c at the first or the second station with the average cell radius R_λ; where $i \in \{1,2\}$
$\hat{P}_{1/2}(i, j; R_\lambda)$	Probability that users are classified into class i at the first and class j at the second station with the average cell radius R_λ
T_1	Upper limit of downlink SINR threshold for class 0 users.
$\bar{\lambda}_{i,c}(R_\lambda)$	Average number of class c users at the first or the second station when the average cell radius is R_λ; where $i \in \{1,2\}$
$\bar{r}_{i,c}$	Channel uses for class c users at the first and second cell; where $i \in \{1,2\}$
$t_{i,c}$	Allocated resources in the time domain for class c users at the first or the second cell where $i \in \{1,2\}$

$f_{i,c}$	Allocated resources in the frequency domain for class c users at the first or the second cell where $i \in \{1,2\}$
B_A	The average active period of a mobile station
B_I	The average idle period of a mobile station
δ	Decoding probability error for URLLC packets
$\lambda_{i,c}(R_\lambda)$	The arrival rate of class c users at the first and second cell with the average cell radius R_λ; where $i \in \{1,2\}$
$N_{i,c}(t)$	The number of class c users at the first and the second cell at time t; where $i \in \{1,2\}$
$\rho_{i,c}(R_\lambda)$	Average load of class c users at the first and second cell at time t; where $i \in \{1,2\}$ and the average cell radius is R_λ
$P_{B,i}(c; R_\lambda)$	The blocking probability experienced by class c users at the first or the second station when the average cell radius is R_λ; where $i \in \{1,2\}$
$P_{B,i}(R_\lambda)$	The average blocking probability experienced by a specific user at the first or the second station when the average cell radius is R_λ; where $i \in \{1,2\}$
$f_{i,j}(x,y)$	Joint PDF of the distance to the first and the second closest stations corresponding to four scenarios in Table 2; where $i \in \{L,N\}$ and j $\in \{L,N\}$
$g_p(x)$	PDF of the distance to the second closest LoS or NLoS station where $p \in \{L,N\}$

$A_{i,j}(R_\lambda)$	The association probability of a typical user connecting to the closest i station, $i \in \{L, N\}$ as a first choice and the second closest j station, $j \in \{L, N\}$ as an alternative option when the average cell radius is R_λ
$\hat{f}_{i,j}(x, y)$	Joint PDF of the distances from the first and the second serving stations to a typical UE as its two available options; where $i \in \{L, N\}$ and j$\in \{L, N\}$
$\hat{g}_p(x)$	PDF of the distance from a typical user to its second closest station as a second serving station; where $p \in \{L, N\}$
$\bar{P}_{C,1/2}(\gamma_1, \gamma_2, R_\lambda)$	The joint SINR coverage probability when at least one downlink SINR at the first or second station is stronger than the target threshold γ_i, $i \in \{1,2\}$ and the average cell radius is R_λ
$P_{B,1/2}(R_\lambda)$	The average probability that a typical user is blocked by both stations where the average cell radius is R_λ

Chapter 1: Introduction

This chapter will introduce the motivation of this dissertation spurred by the challenges of the current mobile network to fulfill the promises of supporting URLLC, a new service category for mission-critical communication. Then, the objectives and contributions are discussed subsequently. Finally, this chapter is concluded by the organization of this dissertation.

1.1 Motivation

The fifth-generation New Radio (5G-NR) aims to support three significant services with various inhomogeneous demands: enhanced mobile broadband (eMBB), massive machine type communications (mMTC), and URLLC. Among the three pillar classes of traffic, URLLC is designed to support a plethora of applications that need high-reliability communication within a strictly bounded transmission time, such as smart factory automation, autonomous vehicles, and virtual reality [1]–[7]. According to the third-generation partnership project (3GPP), URLLC requires a stringent statistical performance guarantee for low delay and high reliability. The typical value of delay constraint is below one millisecond with the packet loss rate below one packet loss in 10^5 packets as mentioned in [8].

Authors in [9], [10] and [11] introduced key enabling mechanisms at different network layers to fulfill URLLC's requirements. First, at physical layers, structure-based mechanisms include a mini-slot frame structure and finite blocklength information theory tailored to URLLC packets. At the same time, diversity-based techniques, including

frequency, time, and space diversities at physical layers, could enhance the reliability of systems aiding URLLC. Next, the pre-emption capability and prioritized scheduling schemes are fundamental mechanisms that reduce latency for URLLC traffic at the link layers. Lastly, cross-layer techniques include spatial diversity of multiple BSs, and hybrid automatic repeat request (HARQ) schemes could be employed to enhance the system robustness that suffices URLLC's requirements.

However, there is very little study on estimating the performance of URLLC traffic using these techniques, which leaves a big gap for deploying URLLC services. Additionally, the performance of URLLC systems utilizing these supporting URLLC techniques depends on both physical and link layer models. Therefore, thoroughly understanding the impacts of combining important factors of physical and link layers on the performance of wireless networks that incorporate key enabling techniques aiding URLLC traffic is essential for designing and deploying advanced wireless networks.

Given the problems and challenges mentioned above, the ultimate goals of this research are discussed in the next section.

1.2 Thesis Objective

Packet loss due to being blocked at a BS which is the unavailability of resources, affects the robustness of the cellular network. Therefore, the average blocking probability plays an important role in evaluating system performance. One of the main focuses of this research is to provide an analytical approach that includes key enabling mechanisms aiding URLLC, and parameters residing at physical and link layers to evaluate the average blocking probability of URLLC users experienced at the serving BS. As a result, this thesis

proposes a novel approach to clarify how dense the wireless system that incorporates enabling mechanisms for URLLC services should be to provide acceptable coverage and mitigate the average blocking probability experienced by mobile stations as much as possible. Moreover, the feasibility of allowing user equipment (UE) to associate with the second closest base station motivated by spatial diversity of multiple BSs, a cross-layer mechanisms for URLLC traffic, is also studied. We want to understand how much improvement the wireless network's overall performance could achieve in terms of coverage and average blocking probability when a second closest base station is also considered.

Next, motivated by the objectives mentioned earlier, the following section presents the contributions of this thesis in detail.

1.3 Contributions

This research explores the possibility of filling the gap between physical and data link layers to establish an analytical approach tailored to cellular networks supporting URLLC services. The key contributions of this thesis can be summarized as follows:

1. We combine physical and data link layers to form a comprehensive analysis to evaluate the blocking probability of the wireless network aiding URLLC. The proposed method analyzes the performance of wireless systems with various enabling mechanisms for URLLC including mini-slot frame structure, finite blocklength and time diversity using packet retransmission based on the HARQ scheme for URLLC packets at physical layers, prioritized scheduling and pre-emption capability of URLLC services at link layers. We derive the analytical

expression of the average blocking probability experienced by an arbitrary URLLC user at the closest base stations as a function of base station density based on concepts from stochastic geometry and queuing theory. To the best of our knowledge, the impact of base station density on the average blocking probability experienced by users has not yet been explored mathematically. Therefore, understanding the effects of network density on the average blocking probability is essential and can be used as a criterion for selecting deployment strategies.

2. By analyzing the numerical results calculated by parameters of millimeter wave (mmWave) systems supporting URLLC services as an example to illustrate our findings, we obtain the cell sizes optimizing the SINR coverage probability and average blocking probability at the closest base station. However, the cell sizes for achieving the two optimal values are not identical, and when we increase the SINR threshold, the difference between them grows further. Thus, optimal cell size should be determined by the average blocking probability based on parameters residing at both link and physical layers rather than considering merely physical layer parameters.
3. Next, we extend our research to study the effect of using multiple base stations inspired by the spatial diversity through different BSs as a cross-layer mechanisms to aid URLLC. In particular, the mathematical expressions for evaluating the joint SINR coverage probability of two closest base stations are derived for a general wireless network. Similarly, analytical expressions calculating the average blocking probability of a mobile station experienced at the second nearest station and both stations are derived while incorporating important factors residing at the

data link and physical layers. More importantly, our approach can be extended to explore the performance of cellular systems that utilize more than two base stations.

4. As a result, we demonstrate how much improvement in terms of reliability of URLLC traffic and the coverage area of the mmWave wireless network, as an example, could enhance when considering the secondary station compared to a single base station. Furthermore, the impact of the densification of the base station on the average blocking probability of the two nearest stations is also investigated. Analogously, the values of cell sizes, which optimize the coverage probability and the average probability that the two nearest stations reject a UE, exist. However, the base station densities achieving optimal SINR coverage and blocking probability values are not identical and more significant than their counterparts at the nearest station using the same SINR thresholds.

Based on the results from our contributions, the network operator can answer several interesting questions: how densely should the deployment be to support URLLC communication under its stringent QoS requirements? What is the average probability that URLLC users are denied service in a given network system? Given the trade-off between the cost and the network performance, is it feasible to utilize the second closest BS?

Additionally, the list of publications resulting from this study is presented in the following subsection.

1.4 Publication List

The research has consequently led to the following publications:

1) Nhat Hieu Le, Changcheng Huang, “Estimating the Blocking Probability for Ultra-Reliable and Low-Latency Communications in Next-Generation Wireless Networks”, *IEEE Vehicular Technology Conference,* Helsinki, June 2022, *under review.*
2) Nhat Hieu Le, Changcheng Huang, “Achieving Ultra-Reliable Low-Latency Communications with Statistical Performance Guarantee for Advanced Wireless Networks”, *IEEE transactions on wireless communications,* January 2022, *under review.*

The outline of this dissertation will be discussed in the section below.

1.5 Thesis Outline

The thesis is organized as follows. Chapter 2 begins with the literature review, relevant description of the technical background to evaluate of the performance of wireless network supporting URLLC services. Additionally, the concise problem statement of this research is mentioned in chapter 2 as well. Next, the blocking probability analysis for the first station is developed in chapter 3. Finally, we apply our proposed approach to perform the coverage analysis using an alternative station in chapter 4. Similarly, chapter 5 evaluates the blocking probability analysis for our novel method. Numerical results are subsequently presented in Chapter 6. Finally, the conclusions and suggestions for future work are mentioned in Chapter 7.

In summary, the challenges in cellular mobile systems that provide URLLC services have been presented in this chapter. Additionally, the current research gap relating to evaluating the performance of wireless systems supporting URLLC services is

highlighted. Furthermore, this dissertation's main objectives and essential contributions have been discussed as well. The following chapter provides the literature survey of related work and prepares the readers with the necessary background to understand the rest of this dissertation.

Chapter 2: Background and Literature Review

This chapter will first introduce a research line that studies the performance of URLLC services. Therefore, we will begin to survey URLLC services and enabling technologies for aiding URLLC first. Since the performance of URLLC depends on both physical and link layer models, without loss of generality, we will study the performance of mmWave networks aiding URLLC services as an example. Consequently, the survey of physical models, where mmWave is used as a special case, will be presented subsequently for calculating the performance of wireless systems. The survey of link layer models for evaluating the blocking probability will be introduced later. Next, system models used in this dissertation, how to calculate the SINR coverage probability, and the generalized Erlang loss model analysis will be discussed in the background section. Finally, this chapter will conclude with the problem statement.

2.1 Literature Review

Surveys about principles and building blocks for supporting URLLC, including key techniques and methodologies, can be found in [2], [9]-[11]. Various interesting enabling techniques, classified as physical and mac layer mechanisms or cross-layers mechanisms to enable URLLC, were explored comprehensively. The enabling technologies at physical layers include flexible frame structure, finite blocklength model, and the utilization of diversity techniques in time, frequency, and space to improve the latency and reliability for URLLC traffic. At link layers, congestion control, prioritized scheduling scheme, and pre-emption capability of URLLC could enhance the performance of wireless systems to

support URLLC. Cross-layers techniques include novel ARQ or HARQ schemes that affect the latency when using packet retransmission. Additionally, multi-connectivity or interface diversity mechanisms were suggested to enhance the reliability of wireless systems. Furthermore, motivated by ultra-dense network setups, user-void BSs that have no associated users could provide alternative associations for URLLC services. This can be considered as the spatial diversity of multiple base stations. Likewise, the physical layer challenges to support URLLC services were surveyed in [12], such as packet structure, fading effects, link budget analysis, and modulation and coding scheme. Besides that, authors in [13] and [14] studied the deployment strategy and suitable modulation and coding scheme to satisfy URLLC's stringent requirements.

Even though orthogonal frequency-division multiple-access (OFDMA) has been officially applied as the access link in LTE networks, a new frame structure is needed to support URLLC service. The 3GPP standards committee proposed a novel OFDMA frame that adopts scalable numerology to accommodate the demanding QoS requirements of URLLC traffic in [15]. Furthermore, mini-slot level access to radio resources was also introduced in which the number of orthogonal frequency-division multiplexed (OFDM) symbols per transmit time interval (TTI) can also vary. Another design challenge of a wireless network that supports URLLC is that, unlike the current cellular system where the traffic packet size and transmission delay are large, the URLLC traffic has finite block-length and low-latency transmission. Thus, Shannon's capacity formula based on the law of large numbers cannot be directly applied [16]. Therefore, the achievable data rate of URLLC traffic needs to be reconsidered.

While eMBB applications can achieve ultra-high reliability by relying on sufficient re-transmission attempts, this approach does not apply to URLLC due to the strict delay constraint. 3GPP recommended a superposition/puncturing framework in [17], and the short TTI approaches in [18] for dynamic multiplexing eMBB and URLLC traffics in 5G network. Various approaches to solving the scheduling and resource allocation aspects of URLLC have been investigated in the literature. The line of work [19]−[21] focused on the joint eMBB and URLLC traffic scheduling to simultaneously fulfill URLLC demands and optimize the spectral efficiency of both services. Logically, dedicating fixed frequency bands to eMBB and URLLC is preferable since it poses minor challenges to system design. However, the authors in [19] showed that it is inefficient in system resource utilization. Instead, a dynamic multiplexing solution should be employed. A recent study in [20] investigated the problem of puncturing in OFDMA systems where URLLC traffic at the mini slot timescale preempts into eMBB allocations. The authors assumed that URLLC packets should be scheduled instantly when the traffic arrives. The main goal is that the broadband traffic should be minimally impacted when maximizing the URLLC outage capacity. The joint optimization of resource allocation for eMBB and URLLC traffic was considered in [21], in which a flexible frame structure and numerology approach are adopted to improve the spectral efficiency of mission critical services. However, the authors did not consider the puncturing/superposition method.

One of the promising enablers for URLLC traffic is the mmWave bands for access links due to the abundant spectrum resources and high transmission rate [22]−[25]. Recent studies suggest that the distinguishing features of mmWave systems typically promise to deliver higher throughput to support exponentially increasing users who require ubiquitous

access to high peak data rates of cellular data [26]. Authors in [27]–[30] explored distinguishing propagation traits of mmWave bands. First, mmWave carrier frequency has an increasing path-losses according to Friis transmission formula. Second, mmWave signals are more sensitive to blockages due to severe penetration loss when it travels through particular materials [28]. Hence, indoor users are unlikely to be covered by outdoor base stations. Third, research in [27] unveiled that the path loss characteristic of line-of-sight (LoS) and non-line-of-sight (NLoS) links varies considerably due to blockages. Therefore, the different features between propagation environments need to be considered to provide a robust system analysis of mmWave cellular networks.

A comprehensive analytical method to evaluate the performance of Sub-6GHz (conventional) cellular networks was established, starting with [31] using stochastic geometry. By modeling the base station locations as Poisson point process (PPP) on the 2D plane, the model provided an asymptotic result of the performance in a real-world cellular system. Unfortunately, the method is not applicable to the mmWave system due to its distinguishing propagation characteristics. Based on this framework, the performance analysis of multi-tier and heterogeneous networks was later studied in [32] and [33]. Unfortunately, the framework to analyze the Sub-6GHz network cannot simply apply to the mmWave network because of the distinguish propagation characteristics of mmWave bands and the usage of directional beamforming.

Stochastic geometry was first used in [34] to evaluate the SINR and rate in mmWave cellular systems. The paper concluded that the mmWave system could provide much higher data rates with competitive coverage than the microwave systems when the link budget is satisfied. Both intra-cell and inter-cell interference were considered, but

blockages and the different LoS and NLoS links were not incorporated in the analysis. The effect of blockages was first analyzed in [35], where arbitrary obstacles in urban cellular networks are modeled by a stochastic framework using random shape theory.

Authors in [36] incorporated the effects of blockage and different propagation characteristics on the mmWave system. The authors developed an analytical stochastic geometry solution to conduct a systematic study of the mmWave cellular network. The SINR distribution was evaluated by assuming BSs be spatially distributed according to PPP. Several exciting takeaways were derived from this paper. First, the results show that mmWave networks have higher coverage and capacity if the base stations are densely deployed. Moreover, the coverage and rate expressions are functions of antenna geometry, densification of the base station network, and the desired SINR threshold. Furthermore, the densification of base stations should not exceed an optimal value, after which the performance of mmWave networks degrades. Intuitively, the serving link distance is reduced when the average cell size decreases. Therefore, the serving base station provides higher power to a typical user. At the same time, the interference term will also increase. When we keep reducing the average cell size smaller than the optimal value, the interference term will be stronger than the increase in the serving power received by a user; thus, the SINR coverage performance will degrade.

In [37] and [38], the authors extended mathematical approaches to study the impact of statistical channels and antenna models on the performance of mmWave networks. An extensive directional antenna arrays model in mmWave networks was studied in [37], and coverage analysis was presented in cellular and ad-hoc networks. In addition, the multi-slope path loss model was employed in [38]. Although the research mentioned above

explored the performance of the mmWave network with various propagation models and antenna techniques, they have not studied the performance under URLLC requirements, which needs to consider both physical and link layers.

In [19], the authors applied queuing theory and conducted simulations to investigate the design of cellular systems to support URLLC communication. Primarily, they explored the fundamental trade-offs between the reliability, system capacity, and the latency requirement for URLLC packets by introducing *M/M/m/k* and *M/D/m/m* queuing models for users at the cell edge. However, the effects of re-transmissions, decoding probability failure, and a finite block-length packet feature were not considered. Adopting the multi-class queuing model, the authors in [39] proposed a simple one-shot transmission scheme to study how resource provisioning in the time-frequency domain affects the system's reliability. The authors then extended the one-shot model to incorporate the HARQ scheme, which allows re-transmissions of URLLC packets. Especially, the guideline on designing a robust wireless network to support URLLC traffic was also provided. However, the paper does not consider how the densification of the cellular network affects the reliability of URLLC communication. However, the paper did not consider how the deployment strategies of the cellular network such as cell sizes, antenna model, and the target SINR threshold affect the overall reliability of the system supporting URLLC service.

The classical Erlang loss model, or *M/M/m/m*, was developed by authors in [40] to evaluate the blocking probability of circuit-switched telephone networks. Calls arrive at the system according to a Poisson process, and the holding times of each call are exponentially distributed. There are *m* lines in total. Calls, upon arrival, do not find

available links are blocked and lost. Meanwhile, the Engset loss model [41], or *M/M/m/m/k*, is obtained by replacing calls generated by a single Poisson process with k circulating sources ($m < k$), also called closed systems. Each source generates a call according to a Poisson process, and then the call either acquires a line for an exponentially distributed holding time or is blocked. Interestingly, the Engset loss model can also be treated as special cases of the Erlang loss model with state-dependent arrival calls related to k sources.

Moreover, the authors in [42] introduced the generalized loss model, either the generalized Erlang loss model or the generalized Engset loss model. For the generalized Erlang loss model, calls are generated from multi-class sources, consisting of total $\mathscr{C}$ classes. Calls originated from class c source require N_c lines and are state-dependent since the subsequent constraint must be satisfied, $\sum_{c=1}^{\mathcal{C}} N_c n_c(t) \leq m$, where $n_c(t)$ denotes the number of class c calls at time t, and m is the total available lines. Moreover, the call holding times are independent and generally distributed. The generalized Engset loss model is a special case of the generalized Erlang loss model where state-dependent arrival rates of class c calls are generated from a limited number of sources, k_c. This research adopts the generalized Erlang loss model to evaluate the system performance.

The system models used in this thesis will be introduced in the next section. Additionally, analytical methods to calculate the SINR coverage probability and the analysis of the generalized Erlang loss model proposed by previous studies will be presented as the foundation for this research subsequently.

2.2 Background

In this section, we will introduce our system model, including network, channel, and antenna models, to analyze the system performance, the SINR coverage probability, at the physical layer of cellular networks under the mmWave bands. Lastly, we will present how the stationary distributions of the state-process in the generalized Erlang loss model is calculated.

2.2.1 Network Model

We adopt assumptions made by [36] to develop our baseline system model for the downlink mmWave cellular network. The critical assumptions are discussed as follows.

Outdoor BSs are assumed to be randomly distributed following a homogeneous PPP $\Phi = \{\boldsymbol{X_i}, i \geq 0\}$ of density λ, where $\boldsymbol{X_i}$ is the location of the i-th base station. Due to the high penetration loss nature of mmWave bands, the interference of indoor BSs is ignored. Outdoor User Equipment (UE) follow a PPP Φ_{u} of density λ_u on the same plane and is independent with outdoor BSs. Each user is assumed to be associated with a base station having the smallest path loss. By the stationary and independence properties of user process, a downlink SINR received by a typical (randomly selected) user located at the origin 0 has an identical distribution of an arbitrary user in the network. The serving base station for a typical user is denoted as $\boldsymbol{X_0}$, $\boldsymbol{R_0} = \|\boldsymbol{X_0}\|$, where $\boldsymbol{R_0}$ is the distance of serving link and $\boldsymbol{R_i} = \|\boldsymbol{X_i}\|, i > 0$ are random variables indicating the link distance from the *i-th* BS to the typical user.

Distributions of BS are split into two independent PPPs corresponding to LoS and NLoS paths by blockages. The LoS probability function is a non-increasing function

defined as $b(r) = e^{-\beta r}$, where r is a link length, and β is a parameter obtaining by the density and the average size of blockages. Consequently, a link of length r is NLoS with a probability $1 - b(r)$. As a result, the LoS and NLoS BSs are distributed based on two independent non-homogenous PPPs Φ_{L} and Φ_{N} with density functions $b(r)\lambda$ and $(1 - b(r))\lambda$, respectively. Subsequently, the next section will introduce the channel model used in this research.

2.2.2 Channel Model

Distinct path loss parameters are applied for LoS/NLoS links. Let α_L and α_N be the path loss exponents for LoS and NLoS links, respectively. The path loss of a link with an arbitrary length r is

$$l(r) = \begin{cases} C_L r^{-\alpha_L} & w.p. \quad b(r) \\ C_N r^{-\alpha_N} & w.p. \quad 1 - b(r) \end{cases} \tag{1}$$

where C_L, C_N are the path loss intercepts and $b(r)$ is the LoS probability function.

The Rayleigh fading model for the conventional networks, predicated on a large amount of local scattering, does not apply to mmWave bands, especially when directional beamforming is used. According to authors in [43], the Nakagami model derived from chi-distribution is a beneficial model to characterize environments with multiple NLoS components, but it cannot characterize LoS components. However, empirical measurements show that small-scale fading has a relatively minor impact in mmWave systems as mentioned in [24] and [44]. Therefore, we assume independent Nakagami fading for each link similar to the fading model in [36], which is more general but still tractable. Different parameters N_L and N_N are assumed for LoS and NLoS paths. Let us

define $\boldsymbol{H_0}$ and $\boldsymbol{H_i}$ be the small-scale fading random variables for the serving and i-th interference links, thus, under Nakagami fading assumption, $|\boldsymbol{H_0}|^2$ and $|\boldsymbol{H_i}|^2$ are normalized Gamma random variables of small-scale fading in signal power. Additionally,

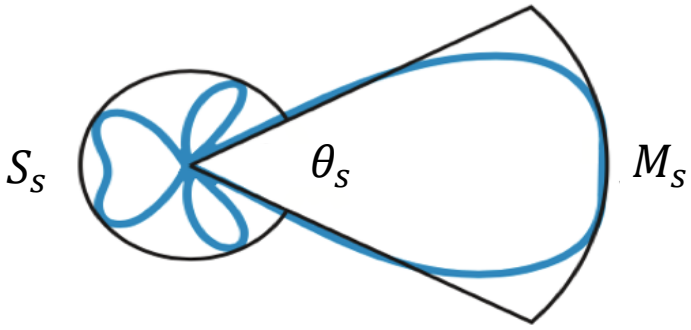

Figure 2-1 Approximated sector antenna model at transmitters and receivers with main-lobe directivity gain, side-lobe directivity gain and half-power beamwidth [36].

we ignore the shadowing effect in our model. Next, the antenna model is presented in the following session.

2.2.3 Antenna Model

In this research, we approximate the actual pattern by the sectored antenna model illustrated in Figure 2-1 as [36]. Our system supports multiple input and multiple output (MIMO) antenna technology since UE and BSs are assumed to be equipped with large directional antenna arrays supporting analog beamforming. The typical user and its serving station are assumed to have perfect channel knowledge and adjust their steering orientations by tuning the weights of phase shifters at antenna arrays of both the receivers

and transmitters to exploit maximum directivity gain. Meanwhile, the steering angles of interference cells are uniformly distributed on the plane.

Let $\boldsymbol{G_i}, i > 0$ be the total directivity gain from a typical user to the interference base station, $\boldsymbol{X_i}$. The directivity gain $\boldsymbol{G_i}$ is a discrete random variable that has the probability mass function, $\boldsymbol{G_i} = A_k$ with probability B_k ($k \in \{1,2,3,4\}$), where A_k and B_k are defined

Table 1 Probability mass function of $\boldsymbol{G_i}$

k	A_k	B_k
1	$M_R M_T$	$C_R C_T$
2	$M_R S_T$	$C_R(1 - C_T)$
3	$S_R M_T$	$(1 - C_R)C_T$
4	$S_R S_T$	$(1 - C_R)(1 - C_T)$

in Table 1. M_i, S_i, θ_i are parameters denoting main lobe directivity gain, back lobe gain, and a half-power beamwidth of the main lobe at transmitters or receivers; $C_R = \frac{\theta_R}{2\pi}$ and $C_T = \frac{\theta_T}{2\pi}$, where $i \in \{T, R\}$, are constants. For the serving link, the maximum directivity gain is defined as $G_0 = M_R M_T$.

Based on this model, the downlinks SINR, $\boldsymbol{\gamma_{D,1}}$ at the first BS received by the typical mobile station which is similar to [36], can be evaluated as follows:

$$\boldsymbol{\gamma_{D,1}} = \frac{|\boldsymbol{H_0}|^2 M_r M_t \, l(\boldsymbol{R_0})}{\sigma^2 + \sum_{i>0:\boldsymbol{X_i}\epsilon\Phi} |\boldsymbol{H_i}|^2 \boldsymbol{G_i} l(\boldsymbol{R_i})} \tag{2}$$

where σ^2 is the normalized thermal noise power, $\boldsymbol{R_i}$ is a random variable that depicts the length of the interference link from UE to the i-th cell. Therefore, the downlink SINR is also a random variable due to the stochasticity of the base station locations, the small-scale

fading, and the directivity gain. Furthermore, as the mobile station and its serving base station can estimate the channels perfectly and error in channel estimation is neglected.

The next session will provide the approach to calculate the SINR coverage probability of mmWave wireless systems.

2.2.4 SINR Coverage Probability Analysis

We now undergo steps to analyze the coverage in our system model of a general mmWave network. We first introduce the definition of the average cell radius which is computed as $R_\lambda = \sqrt{\frac{1}{\pi\lambda}}$, where λ is the density of outdoor base stations. The average cell radius of the network represents the density of the cellular network and decides the inter-site distance. A small average cell size indicates a high BS density in the network.

The SINR coverage probability at the single station $P_{C,1}(\gamma, R_\lambda)$ is that the received SINR is more significant than a predefined threshold γ. As the mobile station can associate with a station either in Φ_L and Φ_{N} which are independent point processes. Hence, we will handle LoS and NLoS cells separately. The serving base station can be the nearest LoS or NLoS cell. Let two random variables $\boldsymbol{R_{L,i}}, \boldsymbol{R_{N,i}}$ be distances to the i-th closest LoS and NLoS stations, and $r_{L,i}, r_{N,i}$ are the observed values of those variables. Note that both $r_{L,i}$ and $r_{N,i}$ are positive values. We will first introduce the following lemmas to derive the SINR coverage probability.

Lemma 1 (Modified from [36, Lemma 1]): The probability density function (PDF) of the distance to the nearest LoS station is calculated by

$$f_L(r_{L,1}; R_\lambda) = 2R_\lambda^{-2} a_L(r_{L,1}) e^{-2R_\lambda^{-2} i_L(0, r_{L,1})}, \tag{3}$$

where $r_{L,1} > 0$. Identically, we can express the PDF of the distance of the nearest NLoS station is

$$f_N(r_{N,1}; R_\lambda) = 2R_\lambda^{-2} a_N(r_{N,1}) e^{-2R_\lambda^{-2} i_N(0, r_{N,1})}, \tag{4}$$

where

$$a_L(x) = xb(x), \tag{5}$$

$$a_N(x) = x\big(1 - b(x)\big), \tag{6}$$

and

$$i_L(x, y) = \int_x^y tb(t)\mathrm{dt}, \tag{7}$$

$$i_N(x, y) = \int_x^y t\big(1 - b(t)\big)dt. \tag{8}$$

We now compute the probability of a typical UE connecting with either a LoS or a NLoS station with the link length distribution from the nearest station in the next lemma.

Lemma 2 (Modified from [36, Lemma 2]): The probability of a UE associating with the nearest LoS base station is

$$A_L(R_\lambda) = \int_0^\infty e^{-2R_\lambda^{-2} i_N\left(0, \psi_L(r_{L,1})\right)} f_L(r_{L,1}; R_\lambda) dr_{L,1}, \tag{9}$$

where $r_{L,1} > 0$ and $\psi_L(r_{L,1}) = \left(\frac{C_N}{C_L}\right)^{1/\alpha_N} {r_{L,1}}^{\alpha_L/\alpha_N}$. Consequently, the probability that a UE associates with the nearest NLoS station is

$$A_N(R_\lambda) = 1 - A_L. \tag{10}$$

Furthermore, the distribution of the distance from a mobile station to its connecting base station is given by the following lemma.

Lemma 3 (Modified from [36, Lemma 3]): The PDF of the link length to the nearest serving LoS station is computed as

$$\hat{f}_L(r_{L,1};R_\lambda) = e^{-2R_\lambda^{-2} i_N\left(0,\psi_L(r_{L,1})\right)} f_L(r_{L,1};R_\lambda), \tag{11}$$

where $r_{L,1} > 0$. Analogously, the PDF of the distance to the closest NLoS station is

$$\hat{f}_N(r_{N,1};R_\lambda) = e^{-2R_\lambda^{-2} i_L\left(0,\psi_N(r_{N,1})\right)} f_N(r_{N,1};R_\lambda), \tag{12}$$

where $r_{N,1} > 0$ and $\psi_N(r_{N,1}) = \left(\frac{C_L}{C_N}\right)^{1/\alpha_L} {r_{N,1}}^{\alpha_N/\alpha_L}$. We will introduce one important theorem to analyze the SINR coverage at a single station based on *Lemma 2* and *Lemma 3* in the next theorem. The SINR coverage probability of the nearest station $P_{C,1}(\gamma_1, R_\lambda)$ is the probability that for a typical user, whose downlink SINR from the closest station $\boldsymbol{\gamma_{D,1}}$ exceeds a threshold γ_1 with the average cell radius is R_λ.

Theorem 1 (Modified from [36, Theorem 1]): The SINR coverage probability can be computed as

$$P_{C,1}(\gamma_1, R_\lambda) = P_{C,L}(\gamma_1, R_\lambda) \; + \; P_{C,N}(\gamma_1, R_\lambda), \tag{13}$$

where $P_{C,S}(.), S \in \{L, N\}$ is the coverage probability given a user connects with a station in Φ_S, and each term can be evaluated as

$$P_{C,L}(\gamma_1, R_\lambda) \;\approx \int_0^\infty p_L(r_{L,1};\gamma_1, R_\lambda)\, \hat{f}_L(r_{L,1};R_\lambda) dr_{L,1}, \tag{14}$$

and

$$P_{C,N}(\gamma_1, R_\lambda) \approx \int_0^\infty p_N(r_{N,1};\gamma_1, R_\lambda)\, \hat{f}_N(r_{N,1};R_\lambda) dr_{N,1}, \tag{15}$$

where

$$p_L(r_{L,1};\gamma_1, R_\lambda)$$

$$\approx \sum_{n=1}^{N_L} (-1)^{n+1} \binom{N_L}{n} e^{-q_1(r_{L,1},n;\gamma_1) - q_2(r_{L,1},n;\gamma_1,R_\lambda) - q_3(r_{L,1},n;\gamma_1,R_\lambda)}, \tag{16}$$

$$p_N(r_{N,1};\gamma_1, R_\lambda)$$

$$\approx \sum_{n=1}^{N_N} (-1)^{n+1} \binom{N_N}{n} e^{-v_1(r_{N,1},n;\gamma_1)-v_2(r_{N,1},n;\gamma_1,R_\lambda)-v_3(r_{N,1},n;\gamma_1,R_\lambda)}, \tag{17}$$

$$q_1(r_{L,1},n;\gamma_1) = \frac{n\sigma^2\eta_L {r_{L,1}}^{\alpha_L}}{C_L M_R M_T}\gamma_1, \tag{18}$$

$$q_2(r_{L,1},n;\gamma_1,R_\lambda) = 2R_\lambda^{-2}\sum_{k=1}^{4} B_k \int_{r_{L,1}}^{\infty} h\left(N_L, \frac{n\eta_L \bar{A}_k {r_{L,1}}^{\alpha_L}}{N_L t^{\alpha_L}}\gamma_1\right) a_L(t)dt, \tag{19}$$

$$\begin{aligned} &q_3(r_{L,1},n;\gamma_1,R_\lambda) \\ &= 2R_\lambda^{-2}\sum_{k=1}^{4} B_k \int_{\psi_L(r_{L,1})}^{\infty} h\left(N_N, \frac{nC_N\eta_L \bar{A}_k {r_{L,1}}^{\alpha_L}}{C_L N_N t^{\alpha_N}}\gamma_1\right) a_N(t)dt, \end{aligned} \tag{20}$$

$$v_1(r_{N,1},n;\gamma_1) = \frac{n\sigma^2\eta_N {r_{N,1}}^{\alpha_N}}{C_N M_R M_T}\gamma_1, \tag{21}$$

$$\begin{aligned} &v_2(r_{N,1},n;\gamma_1,R_\lambda) \\ &= 2R_\lambda^{-2}\sum_{k=1}^{4} B_k \int_{\psi_N(r_{N,1})}^{\infty} h\left(N_L, \frac{nC_L\eta_N \bar{A}_k {r_{N,1}}^{\alpha_N}}{C_N N_L t^{\alpha_L}}\gamma_1\right) a_L(t)dt, \end{aligned} \tag{22}$$

$$v_3(r_{N,1},n;\gamma_1,R_\lambda) = 2R_\lambda^{-2}\sum_{k=1}^{4} B_k \int_{r_{N,1}}^{\infty} h\left(N_N, \frac{n\eta_N \bar{A}_k {r_{N,1}}^{\alpha_N}}{N_N t^{\alpha_L}}\gamma_1\right) a_N(t)dt, \tag{23}$$

and $h(v,x) = 1 - \frac{1}{(1+x)^v}$. For $S \in \{L,N\}, \eta_S = N_S(N_S!)^{\frac{-1}{N_S}}$, N_s are Nakagami small-scale fading parameters. Additionally, $\bar{A}_k = \frac{A_k}{M_R M_T}, k \in \{1,\dots,4\}$ where A_k and B_k are the probabilities and the directivity gain constants defined in Table 1.

The following section presents the approach to analyze the stationary distribution of the generalized Erlang loss model.

2.2.5 Analysis of the Generalized Erlang Loss Model

Let a set, $\mathcal{C}$ denote all call classes, and calls from class *c* follow a Poisson process with the rate λ_c to circuit-switched telephone networks. Moreover, let $n_c(t)$ denote the number of class *c* calls at time *t,* and N is the total available lines. A class c call acquires

N_c lines in total, and there is a constraint that needs to be met, $\sum_{c=1}^{\mathcal{C}} N_c n_c(t) \leq N$. The class *c* call holding time follows the general distribution with the mean $1/\mu_c$. Let the state of the generalized Erlang loss model be denoted by vector $\boldsymbol{n}(t) = (n_c(t) : c \in \mathcal{C})$. The following lemma evaluates the stationary distribution of state-process in the generalized Erlang loss model.

Lemma 4 (Modified from [42, Theorem 2.1]): The stationary distribution of the state-process $\boldsymbol{n}(t)$ in the generalized Erlang loss model is given by

$$P(\boldsymbol{n}|N) = \frac{\prod_{c=1}^{\mathcal{C}} \left(\frac{\rho_c^{n_c}}{n_c!}\right)}{\sum_{\boldsymbol{n}\epsilon \boldsymbol{S}} \prod_{c=1}^{\mathcal{C}} \left(\frac{\rho_c^{n_c}}{n_c!}\right)}, \tag{24}$$

where $\rho_c = \lambda_c/\mu_c$, and $\boldsymbol{S}$, which is the set of feasible states, is given by

$$\boldsymbol{S} = \{\boldsymbol{n} \geq \boldsymbol{0} \mid \sum_{c=1}^{\mathcal{C}} N_c n_c(t) \leq N\}. \tag{25}$$

Subsequently, the following section will introduce concise descriptions of the issues that motivated this research that requires addressing.

2.3 Problem Statement

Given the stringent statistical performance guarantee for ultra-reliable and low delay of URLLC packets, thoroughly understanding is required to systematically analyze and estimate the performance of wireless systems supporting URLLC services. However, according to the studies mentioned above, there is little work on estimating wireless systems' performance that utilizes both crucial aspects of the physical and link layers while incorporating different techniques supporting URLLC services. Therefore, this thesis focuses on combining physical and link layers to estimate a wireless system's performance

with URLLC key enabling techniques, including packet retransmission, radio resource allocation, scheduling schemes for URLLC packets, and spatial diversity through different base stations.

Chapter 3: Blocking Probability Analysis for a Single Station

This chapter will estimate the average blocking probability of a particular user experienced when connecting to the nearest station. A wireless packet is susceptible to various factors that can corrupt or lose data in transit. When a base station with a scarce resource cannot accommodate UE's requests, that user is blocked, so the packet is lost. Consequently, minimizing the blocking probability improves the reliability, and it is necessary to analyze the blocking probability at a particular station that a mobile station suffers on average. Additionally, both physical and link layers are combined to estimate the performance of wireless systems that have supporting technologies of URLLC services. Our models include enabling mechanisms to support URLCC such as time diversity mechanisms that utilize packet retransmission based on HARQ scheme, flexible frame-structure, and finite blocklength model for URLLC packets. Furthermore, prioritized scheduling schemes and pre-emption capability for URLLC services are also considered in our model.

3.1 Data Link Model

Outdoor base stations are randomly located on the plane following a homogeneous PPP process with density λ. Likewise, outdoor users are distributed as a stationary point process with a density λ_u independent of the base stations and blockages. Moreover, the URLLC users' packets have stringent requirements in that a transmission of size L bits must be transmitted successfully within the total delay of D with packet loss rate Δ. We will

consider a scenario where the total bandwidth available for URLLC services at each station is W Hz.

This thesis focuses on URLLC traffic with the highest priority that can pre-empt lower priority traffic, and only control messages have higher priority than URLLC traffic. Typically, the control traffic consumes very little resource; thus, lower-priority traffic and control messages has no impact on the blocking probability of URLLC users. We assume that upon arrival by superposition/puncturing framework, URLLC packets are scheduled instantly or dropped, and the new packets do not pre-empt an ongoing URLLC transmission. URLLC downlink traffic could be transmitted during an ongoing eMBB transmission. To satisfy the latency constraints, URLLC packets cannot be queued until the next slot. Instead, each eMBB slot is divided into mini-slots. Thus, URLLC demand can be immediately scheduled upon arrival in the next mini-slot on top of the ongoing eMBB transmission. If the BS chooses non-zero transmission powers for both eMBB and overlapping URLLC traffic, this is called superposition. If eMBB transmissions are allocated zero power when URLLC traffic is overlapped, it is called puncturing eMBB transmissions. Therefore, our model includes flexible frame structure, prioritized scheduling, and pre-emption capability mechanisms, which are considered as key techniques to enable URLLC.

Additionally, each user receives bursts of packets with active periods b_A and idle periods b_I following exponential distributions. During the busy periods, users wake up, listen, and receive bursts of URLLC packets from its associating station that may include re-transmissions. Moreover, in this research, we consider downlink transmission of URLLC traffic in a Frequency Division Duplex (FDD) based system with dedicated

frequency bands for uplink and downlink. Additionally, HARQ schemes are incorporated so that a URLLC packet is allowed up to M_c transmission attempts. Wireless traffic is susceptible to various factors that can corrupt or lose data in transit. Hence, it is reasonable to assume that a base station will refuse to provide services for users whose SINRs are below a predefined threshold.

The following section will introduce the distribution of user classes at the closest base station based on the result of SINR coverage probability in section 2.2.4.

3.2 Distributions of User Classes

We assume that given the deployment of base stations, the cell coverage area forms a Voronoi diagram covering all users for whom the base station is the nearest. As outdoor users are distributed as PPP, the average number of users falling in each cell follows the PPP distribution with density $\bar{\lambda} = \frac{\lambda_u}{\lambda}$.

It is impossible to calculate the blocking probability of a mobile station for the continuous system using the generalized Erlang loss models in [42]. Therefore, we shall consider the multi-class system that assigns users into $\mathcal{C}$ classes where each class denotes users sharing the same SINR range.

We, hereafter, quantizes downlink SINRs of mobile stations into multiple segments that are $[T_1, T_2), \dots, [T_c, T_{c+1}), \dots, [T_{\mathcal{C}}, \infty)$ where the c-th SINR segment $[T_c, T_{c+1})$ includes all users whose the downlink SINRs are between T_c and T_{c+1}. The probability that a specific user is assigned into class c can be expressed as

$$\hat{P}_{C,1}(c; R_\lambda) = P_{C,1}(T_c; R_\lambda) - P_{C,1}(T_{c+1}; R_\lambda), \tag{26}$$

where $P_C(.)$ is computed in (13) as the SINR coverage probability. Meanwhile, class 0 users include mobile stations that downlink SINR is below T_1, and are rejected by the closest serving BS due to unstable connection. As a result, the blocking probability is always one.

The average number of users that are assigned into class c in the nearest station is defined as

$$\bar{\lambda}_{1,c}(R_\lambda) = \bar{\lambda}\,\hat{P}_{C,1}(c; R_\lambda) \tag{27}$$

Moreover, one critical aspect which needs thoughtful consideration is how resource provisioning is conducted for URLLC transmissions. We assume that our wireless models are OFDMA based; hence users' packets are transmitted in time-frequency.

3.3 Resource Requirements to Transmit URLLC Codewords

A URLLC packet of L information bits destined to a class c user requires r_c channel uses from the serving station in the time-frequency domain to send its codewords. Our system employs the finite blocklength mechanism, one of the key techniques to enable URRLC, to determine resource allocations for URLLC packets. We reuse the results explored by [39] for the finite blocklength regime. In AWGN channel, L information bits that could be transmitted in r channel uses given the received SINR, γ and δ, the decoding probability error of the codeword, is given by

$$L = rn(\gamma) - Q^{-1}(\delta)\sqrt{r\bar{n}(\gamma)} + 0.5log_2(r) + O(1), \tag{28}$$

where $n(x) = log_2(1+x), Q(.)$ is the Q-function, $\bar{n}(x) = (log_2(e))^2(1-(1+x)^{-2})$, δ is the decoding probability error, and $O(.)$ is a big-O notation.

Based on (28), at the closest station, the channel uses for class c users, with the downlink SINR $\gamma_{1,c}$ for a single transmission is approximately by

$$\bar{r}_{1,c} \approx \frac{L}{n(\gamma_{1,c})} + \frac{(Q^{-1}(\delta))^2 \bar{n}(\gamma_{1,c})}{2(n(\gamma_{1,c}))^2} + \frac{(Q^{-1}(\delta))^2 \bar{n}(\gamma_{1,c})}{2(n(\gamma_{1,c}))^2} \sqrt{1 + \frac{4Ln(\gamma_{1,c})}{\bar{n}(\gamma_{1,c})(Q^{-1}(\delta))^2}}, \quad (29)$$

The proof is straightforward as (29) is an approximate solution of (28), a quadratic equation in $\sqrt{r}$ when we ignore $0.5log_2(r)$ and $O(1)$ terms. Hence, it is skipped here.

URLLC packets destined to class c users are allocated with a bandwidth of $f_{1,c}$ for a period $t_{1,c}$ for a single shot transmission. The relationship between the allocated resources in the time-frequency domain with the channel uses is bounded by

$$f_{1,c} = \frac{\bar{r}_{1,c}}{\varepsilon t_{1,c}}, \quad (30)$$

where ε is a scalar denoting the number of channel uses per unit time per unit bandwidth of the OFDMA time-frequency plane. It depends on the OFDMA frame structure and numerology. The bandwidth requirement for all users' URLLC packets will be discussed in the next section.

3.4 Bandwidth Constraint for the Nearest Base Station

Each class c user will use the bandwidth of h_c for an active interval b_A and will stay inactive for a period b_I, assuming $B_A = \mathbb{E}[b_A]$ and $B_I = \mathbb{E}[b_I]$ are the average active and idle period, respectively. We shall make an important assumption that while users can leave or join a particular cell simultaneously, the average number of users at a certain period is fixed with the rate that equals the density of the PPP of the number of users falling under the base station. Therefore, the number of active users is governed by the Poisson Process

with the arrival rate or the average number of active class c users per millisecond will be calculated as

$$\lambda_{1,c}(R_\lambda) = \frac{B_A}{B_A + B_I} \bar{\lambda}_{1,c}(R_\lambda) \tag{31}$$

Let $N_{1,c}(t)$ denotes the number of class c users at time t. Therefore, we can consider that $\lambda_{1,c} = \mathbb{E}\left[N_{1,c}(t)\right]$. Furthermore, the average load of class c users in the closest station is defined as

$$\rho_{1,c}(R_\lambda) = \lambda_{1,c}(R_\lambda) B_A \tag{32}$$

To simplify the calculation of the blocking probability of users accessing their closest stations, we assume that a station serves the users for whom the station is nearest with highest priority. This assumption allows us to calculate the blocking probability for these users without considering users for whom the station is not closest. The situation of class c users being blocked for accessing their first station will be

$$f_{1,c} + \sum_{\tilde{c}=1}^{\mathcal{C}} f_{1,\tilde{c}} N_{1,\tilde{c}}(t) > W \tag{33}$$

Let us define $\boldsymbol{f}_1 = \left(f_{1,1}, f_{1,2}, \ldots, f_{1,\mathcal{C}}\right)$ that is a vector that includes allocated bandwidths for all classes at the closest station. The constraints for the total delay and transmission time when incorporating HARQ schemes to support re-transmissions will be discussed in the subsequent section.

3.5 Delay Bound under HARQ

This section will study the delay bound of URLLC packets when our model incorporates the time diversity mechanism, one of the key techniques to enable URLLC, using packet retransmission based on the HARQ scheme for URLLC packets. A base

station can allow up to M_c re-transmission attempts to class c users. However, the total delay must be within D seconds, and the reliability of the transaction must be $1-\Delta$ according to the requirement of URLLC. After every transmission, the intended receiver sends one-bit feedback to the base station indicating the success/failure status of the packet decoding process. Suppose that the uplink channel is well provisioned so that there are no scheduling and channel access delays. Therefore, the maximum feedback delay denoted by D_c for class c user includes only the processing and propagation delay at the closest cell. The upper delay bound is given by $\sum_{m=1}^{M_c} t_{1,c,m} + M_c D_c = D$, where $t_{1,c,m}$ is the allocated interval in the time domain for the m^{th} re-transmission of a URLLC packet from the closest station to an arbitrary class c user. Furthermore, we assume that the base station assigns the identical interval for each attempt, $t_{1,c,m} = t_{1,c}$.

Hence, the transmission interval of class c user is bounded by

$$t_{1,c} = \frac{D}{M_c} - D_c. \tag{34}$$

The blocking probability of class c user is given in the next section.

3.6 Blocking Probability at the Closest Base Station

Based on the generalized Erlang loss models for multi-class system, the probability that class c users are rejected is calculated in the below lemma.

Lemma 5: The blocking probability experienced by a class c UE can be formulated as

$$P_{B,1}(c;R_\lambda)=\frac{\sum_{\boldsymbol{n_1}\epsilon \boldsymbol{S_{1,c}}}\prod_{\tilde{c}=1}^{\mathcal{C}}\left(\frac{\rho_{1,\tilde{c}}(R_\lambda)^{n_{1,\tilde{c}}}}{n_{1,\tilde{c}}!}\right)}{\sum_{\boldsymbol{n_1}\epsilon \boldsymbol{S_1}}\prod_{\tilde{c}=1}^{\mathcal{C}}\left(\frac{\rho_{1,\tilde{c}}(R_\lambda)^{n_{1,\tilde{c}}}}{n_{1,\tilde{c}}!}\right)}, \tag{35}$$

where the vector $\boldsymbol{n}_1=(n_1,n_2,\dots,n_{\mathcal{C}})$ denotes the number of active users for each class, $\boldsymbol{S_1}=\{\boldsymbol{n}_1 \mid \boldsymbol{f}_1\boldsymbol{n}_1{}^{\boldsymbol{T}}\le W\}$, $\boldsymbol{f}_1=(f_1,f_2,\dots,f_{\mathcal{C}})$ is a vector that includes allocated bandwidths for all classes at the closest station, and $\boldsymbol{S_{1,c}}=\{\boldsymbol{n}_1 \mid \boldsymbol{n}_1\in \boldsymbol{S_1}, \boldsymbol{n}_1+\boldsymbol{e_c}\notin \boldsymbol{S_1}\}$, where $\boldsymbol{e_c}$ is a unit vector with only a non-zero element at c^{th} position. The proof of this lemma is straightforward and is based on the result from *Lemma 4*.

Next, we will compute the average probability that a typical user is rejected by its serving station in the following section.

3.7 Average Probability at the First Base Station

Based on *Lemma 5*, we now express the analytical likelihood that a specific mobile station suffers a URLLC service interruption on average in the following theorem.

Theorem 2: The average blocking probability of an arbitrary UE experiences at the nearest station, is

$$P_{B,1}(R_\lambda)=\sum_{c=0}^{\mathcal{C}}P_{B,1}(c;R_\lambda)\hat{P}(c;R_\lambda), \tag{36}$$

where $P_{B,1}(0,R_\lambda)$ is always be one since class 0 users are considered blocked by their closest station.

Proof: The proof is straightforward using the law of total probability theorem and then therefore is omitted.

Consequently, this chapter has provided a systematic approach to evaluate the average blocking probability of the mmWave mobile network that has key enabling

techniques supporting URLLC traffic, such as packet retransmission and radio resource allocation for a URLLC packet. The approach considers not only parameters at physical and data layers but stringent requirements for URLLC packets are also incorporated. Furthermore, to explore the benefits of spatial diversity of multiple base stations, the next chapter will explore the coverage performance of the wireless networks in which users could associate with their second closest base stations.

Chapter 4: Coverage Analysis of the Two Closest Base Stations

This chapter will investigate the benefits of space diversity mechanisms, classified as cross-layer techniques, one of the key mechanisms to enable URLLC. Motivated by ultra-dense deployments of next-generation networks, by exploiting the spatial diversity provided by neighbor cells, users can seek alternative services from nearby base stations when their first stations cannot accommodate URLLC traffics for them. Specifically, without loss of generality, we consider the influence of the second mmWave BSs, as an example. There are four independent scenarios in total, as depicted in Table 2. Thus, we will examine each case separately. To determine the two nearest BSs, users could utilize localization techniques such as time of arrival estimations or received signal strength estimations which are roughly accurate as mentioned in [45] and [46]. Based on the received signal strength, for some users, the second BS may be closer than the first BS as the received signal depends not only on the link distance but also on the environment, such as blockages that may affect the received signal. However, on average, the distance to the second base station is larger than the distance to the first station for a typical user. Our calculations are based on average behavior. Alternatively, users and base stations' locations could be shared during the initial access procedure via GPS locations. Moreover, LoS and NLoS BSs to a typical user could be classified based on the statistical characteristics of radio propagation or using machine learning techniques as proposed in [47] and [48]. Although in this section, we consider only the second nearest station, the proposed method can be generalized to evaluate the coverage performance of the network utilizing more than

two stations. First, we will analyze the distribution of distances of the second closest station to a typical user in the following section.

4.1 Distributions of Distances to the Two Closest Base Stations

The following lemma provides the joint distribution of distances from the two nearest stations to a typical user.

Lemma 6: The joint PDF of the distances from a typical user to the first and second closest base stations, which are the two nearest LoS stations, is

$$f_{L,L}(r_{L,1}, r_{L,2}; R_\lambda) = \left(2R_\lambda^{-2}\right)^2 a_L(r_{L,1}) a_L(r_{L,2}) e^{-2R_\lambda^{-2} i_L(0, r_{L,2})}, \quad (37)$$

where $0 < r_{L,1} < r_{L,2}$ are the distances to the closest and the second closest LoS stations, respectively, and $a_L(.), i_L(.)$ are equations defined in (5) and (7). Analogously, the probability density function of the link lengths to the two nearest NLoS stations is

$$f_{N,N}(r_{N,1}, r_{N,2}; R_\lambda) = \left(2R_\lambda^{-2}\right)^2 a_N(r_{N,1}) a_N(r_{N,2}) e^{-2R_\lambda^{-2} i_N(0, r_{N,2})}, \quad (38)$$

where $0 < r_{N,1} < r_{N,2}$ are the distances to the closest and the second closest NLoS stations in that given order, and $a_N(.), i_N(.)$ are defined in (6) and (8).

Table 2 Scenarios of the two closest base stations

	First Station	Second Station
Scenario A	The closest LoS	The second closest LoS
Scenario B	The closest NLoS	The second closest NLoS
Scenario C	The closest LoS	The second Closest NLoS
Scenario D	The closest NLoS	The second Closest LoS

Furthermore, the PDF of the distances of the last two scenarios in Table 2 can be presented as

$$f_{L,N}(r_{L,1}, r_{N,2}; R_\lambda) = \left(2R_\lambda^{-2}\right)^2 a_L(r_{L,1}) a_N(r_{N,2}) e^{-2R_\lambda^{-2} i_L(0, r_{L,1})} \times \left(2R_\lambda^{-2} i_N(0, r_{N,2}) e^{-2R_\lambda^{-2} i_N(0, r_{N,2})} - e^{-2R_\lambda^{-2} i_N(0, r_{N,2})} + e^{-2R_\lambda^{-2} i_N(0,\infty)}\right), \quad (39)$$

and

$$f_{N,L}(r_{N,1}, r_{L,2}; R_\lambda) = \left(2R_\lambda^{-2}\right)^2 a_N(r_{N,1}) a_L(r_{L,2}) e^{-2R_\lambda^{-2} i_N(0, r_{N,1})} \times \left(2R_\lambda^{-2} i_L(0, r_{L,2}) e^{-2R_\lambda^{-2} i_L(0, r_{L,2})} - e^{-2R_\lambda^{-2} i_L(0, r_{L,2})} + e^{-2R_\lambda^{-2} i_L(0,\infty)}\right), \quad (40)$$

where $r_{L,1} > 0$ and $r_{N,1} > 0$ in (40) and $r_{L,2} > 0$ and $r_{N,1} > 0$ in (41).

Proof: The distance from the second nearest LoS cell to a typical user located at the origin O must be greater than that from the closest LoS station, implying that $0 < r_{L,1} \leq r_{L,2}$. Additionally, we define $\left(E_{(0,r_{L,1})}, \tilde{E}_{(r_{L,1},r_{L,2})}, \hat{E}_{(r_{L,2},\infty)}\right)$ as an event in which the distance of the second nearest LoS cell goes beyond $r_{L,2}$. If there is no LoS cell within distance $r_{L,1}$ represented by $E_{(0,r_{L,1})}$, there is one station between $r_{L,1}$ and $r_{L,2}$ denoted by an event $\tilde{E}_{(r_{L,1},r_{L,2})}$ and there is at least one station beyond $r_{L,2}$ as $\hat{E}_{(r_{L,2},\infty)}$. The joint CCDF of the distances from the two nearest LoS stations can be computed as

$$C_{L,L}(r_{L,1}, r_{L,2}; R_\lambda) = \mathbb{P}\left(E_{(0,r_{L,1})}, \tilde{E}_{(r_{L,1},r_{L,2})}, \hat{E}_{(r_{L,2},\infty)}; R_\lambda\right)$$

$$\overset{(a)}{=} \mathbb{P}\left(E_{(0,r_{L,1})}; R_\lambda\right) \mathbb{P}\left(\tilde{E}_{(r_{L,1},r_{L,2})}; R_\lambda\right) \mathbb{P}\left(\hat{E}_{(r_{L,2},\infty)}; R_\lambda\right)$$

$$= e^{-2R_\lambda^{-2} i_L(0,r_{L,1})} \left(2R_\lambda^{-2} i_L(r_{L,1}, r_{L,2})\, e^{-2R_\lambda^{-2} i_L(r_{L,1},r_{L,2})}\right)\left(1 - e^{-2R_\lambda^{-2} i_L(r_{L,2},\infty)}\right)$$

$$= 2R_\lambda^{-2} i_L(r_{L,1}, r_{L,2}) e^{-2R_\lambda^{-2} i_L(0,r_{L,2})}\left(1 - e^{-2R_\lambda^{-2} i_L(r_{L,2},\infty)}\right)$$

$$= 2R_\lambda^{-2} i_L(r_{L,1}, r_{L,2})\left(e^{-2R_\lambda^{-2} i_L(0,r_{L,2})} - e^{-2R_\lambda^{-2} i_L(0,\infty)}\right),$$

where (a) follows the independent properties of PPP of disjoint regions. Hence, the joint PDF of the distances from the two nearest LoS base stations is

$$f_{L,L}(r_{L,1}, r_{L,2}; R_\lambda) = \frac{\partial^2}{\partial r_{L,1} \partial r_{L,2}} C_{L,L}(r_{L,1}, r_{L,2}; R_\lambda)$$

$$= \frac{\partial}{\partial r_{L,1}} \Big[2R_\lambda^{-2} a_L(r_{L,2}) \left(e^{-2R_\lambda^{-2} i_L(0, r_{L,2})} - e^{-2R_\lambda^{-2} i_L(0,\infty)} \right)$$

$$+ 2R_\lambda^{-2} i_L(r_{L,1}, r_{L,2}) \left(-2R_\lambda^{-2} a_L(r_{L,2}) \right) e^{-2R_\lambda^{-2} i_L(0, r_{L,2})} \Big]$$

$$= \left(2R_\lambda^{-2}\right)^2 a_L(r_{L,1}) a_L(r_{L,2}) e^{-2R_\lambda^{-2} i_L(0, r_{L,2})}$$

Similarly, the derivation of the remaining scenarios C and D can follow the same manner and is based on the fact that LoS and NLoS PPP processes are independent. Next, the distribution of the distances from the second nearest station to a typical user will be derived in the next section.

4.2 Distributions of the Distance to the Second Closest Station

The PDF of the distance from the second closest station to a typical user can be evaluated as a marginal distribution of the joint PDF distances of the two closest stations.

Corollary 1: The PDF of the distance of the second nearest LoS station is defined as follows

$$g_L(r_{L,2}; R_\lambda) = \int_0^{r_{L,2}} f_{L,L}(r_{L,1}, r_{L,2}; R_\lambda) dr_{L,1} + \int_0^{\infty} f_{N,L}(r_{N,1}, r_{L,2}; R_\lambda) dr_{N,1}, \quad (41)$$

where $r_{L,2} > 0$. Analogously, the PDF of the distance of the second nearest NLoS station is

$$g_N(r_{N,2}; R_\lambda) = \int_0^{r_{N,2}} f_{N,N}(r_{N,1}, r_{N,2}; R_\lambda) dr_{N,1} + \int_0^{\infty} f_{L,N}(r_{L,1}, r_{N,2}; R_\lambda) dr_{L,1}, \quad (42)$$

where $r_{N,2} > 0$.

The association probability when a typical user is associated with the two nearest base stations will be analyzed in the next section.

4.3 Association Probability Analysis of Two stations

The association probabilities for all the mutually exclusive scenarios in Table 2 are calculated in the following lemma.

Lemma 7: The association probability in which a UE connects with the nearest LoS station as the first choice and the second nearest LoS station as the second choice is

$$A_{L,L}(R_\lambda) = \iint_{r_{L,1}=0, r_{L,2}=r_{L,1}}^{\infty} e^{-2R_\lambda^{-2}\left(i_N\left(0,\psi_L(r_{L,1})\right)+i_N\left(0,\psi_L(r_{L,2})\right)\right)} f_{L,L}(r_{L,1}, r_{L,2}) dr_{L,2} dr_{L,1}, \quad (43)$$

where $0 < r_{L,1} < r_{L,2}$. Similarly, the association probabilities for the last three scenarios are evaluated as

$$A_{N,N}(R_\lambda) = \iint_{r_{N,1}=0, r_{N,2}=r_{N,1}}^{\infty} e^{-2R_\lambda^{-2}\left(i_L\left(0,\psi_N(r_{N,1})\right) + i_L\left(0,\psi_N(r_{N,2})\right)\right)} f_{N,N}(r_{N,1}, r_{N,2}) dr_{N,2} dr_{N,1}, \quad (44)$$

where $0 < r_{N,1} < r_{N,2}$, and

$$A_{L,N}(R_\lambda) = \iint_{r_{L,1}=0, r_{N,2}=\psi_L(r_{L,1})}^{\infty} e^{-2R_\lambda^{-2}\left(i_N\left(0,\psi_L(r_{L,1})\right)+i_L\left(0,\psi_N(r_{N,2})\right)\right)} f_{L,N}(r_{L,1}, r_{N,2}) dr_{N,2} dr_{L,1}, \quad (45)$$

where $0 < r_{L,1}$ and $\psi_L(r_{L,1}) < r_{N,2}$. For the last scenario, the UE's first choice is the NLoS station, and an alternative option is the LoS cell. The association probability of the last scenario in Table 2 is computed as

$$A_{N,L}(R_\lambda) = 1 - A_{L,L}(R_\lambda) - A_{L,N}(R_\lambda) - A_{N,N}(R_\lambda), \tag{46}$$

Proof: A UE can connect with the nearest and the second nearest LoS base station as its first and alternative stations if the second closest LoS cell has smaller signal attenuation than the second nearest NLoS station. Let $L_{L,L}$ be an event where path losses from the two nearest LoS stations are smaller than path losses from the two nearest NLoS cells. The association probability for scenario A is

$$A_{L,L}(R_\lambda) = \mathbb{P}(L_{L,L}; R_\lambda) = \mathbb{P}\left(\left(C_L \boldsymbol{R}_{\boldsymbol{L,1}}^{-\alpha_L} > C_N \boldsymbol{R}_{\boldsymbol{N,1}}^{-\alpha_N}\right), \left(C_L \boldsymbol{R}_{\boldsymbol{L,2}}^{-\alpha_L} > C_N \boldsymbol{R}_{\boldsymbol{N,2}}^{-\alpha_N}\right); R_\lambda\right)$$

$$= \mathbb{P}\left(\left(\boldsymbol{R}_{\boldsymbol{N,1}}^{\alpha_N} > \frac{C_N}{C_L} \boldsymbol{R}_{\boldsymbol{L,1}}^{\alpha_L}\right), \left(\boldsymbol{R}_{\boldsymbol{N,2}}^{\alpha_N} > \frac{C_N}{C_L} \boldsymbol{R}_{\boldsymbol{L,2}}^{\alpha_L}\right); R_\lambda\right)$$

$$= \mathbb{P}\left(\left(\boldsymbol{R}_{\boldsymbol{N,1}} > \psi_L(\boldsymbol{R}_{\boldsymbol{L,1}})\right), \left(\boldsymbol{R}_{\boldsymbol{N,2}} > \psi_L(\boldsymbol{R}_{\boldsymbol{L,2}})\right); R_\lambda\right)$$

$$= \mathbb{P}\left(\Phi_N \cap \mathcal{B}\left(0, \psi_L(\boldsymbol{R}_{\boldsymbol{L,1}})\right) = \emptyset; R_\lambda\right) \mathbb{P}\left(\Phi_N \cap \mathcal{B}\left(0, \psi_L(\boldsymbol{R}_{\boldsymbol{L,2}})\right) = \emptyset; R_\lambda\right),$$

where the last equation indicates that the mobile station associates with the two nearest LoS stations if there is no NLoS station within the distance of $\psi_L(\boldsymbol{R}_{\boldsymbol{L,1}})$ and there is no NLoS station within a circular region of raidus $\psi_L(\boldsymbol{R}_{\boldsymbol{L,2}})$ as well. Since events in the second closest station are independent of those in the closest station the LoS association probability for scenario A can be expressed as

$$A_{L,L}(R_\lambda) = \iint_{r_{L,1}=0, r_{L,2}=r_{L,1}}^{\infty} \mathbb{P}(L_{L,L}; R_\lambda | \boldsymbol{R}_{\boldsymbol{L,1}} = r_{L,1}, \boldsymbol{R}_{\boldsymbol{L,2}} = r_{L,2}) \times f_{L,L}(r_{L,1}, r_{L,2}) dr_{L,2} dr_{L,1}$$

$$= \iint_{r_{L,1}=0, r_{L,2}=r_{L,1}}^{\infty} e^{-2R_\lambda^{-2} i_N\left(0, \psi_L(r_{L,1})\right)} e^{-2R_\lambda^{-2} i_N\left(0, \psi_L(r_{L,2})\right)} \times f_{L,L}(r_{L,1}, r_{L,2}) dr_{L,2} dr_{L,1},$$

where $0 < r_{L,1} < r_{L,2}$ and $f_{L,L}(.)$ is the joint PDF of the distances to the first and second closest LoS stations in (37). Additionally, the joint association probabilities for each scenario defined in Table 2 are bounded by

$$A_L(R_\lambda) = A_{L,L}(R_\lambda) + A_{L,N}(R_\lambda), \tag{47}$$

and

$$A_N(R_\lambda) = A_{N,L}(R_\lambda) + A_{N,N}(R_\lambda), \tag{48}$$

where $A_L(R_\lambda)$, $A_N(R_\lambda)$ are calculated in (9) and (10) respectively. Next, the joint distribution of the distances from a typical user to its serving stations will be derived in the below section.

4.4 Distributions of Distances to Serving Stations

The joint distribution of the distances from the user to its closest serving station as its first choice and its second closest serving station as an alternative option is given in the following lemma.

Lemma 8: The joint PDF of the distances from the serving stations in scenario A to a typical user is given by

$$\begin{aligned} &\hat{f}_{L,L}\left(r_{L,1}, r_{L,2}; R_\lambda\right) \\ &= e^{-2R_\lambda^{-2}\left(i_N\left(0,\psi_L(r_{L,1})\right)+i_N\left(0,\psi_L(r_{L,2})\right)\right)} f_{L,L}\left(r_{L,1}, r_{L,2}\right), \end{aligned} \tag{49}$$

where $0 < r_{L,1} < r_{L,2}$. Analogously, the joint PDF for the remaining scenarios can be expressed as

$$\begin{aligned} &\hat{f}_{N,N}\left(r_{N,1}, r_{N,2}; R_\lambda\right) \\ &= e^{-2R_\lambda^{-2}\left(i_L\left(0,\psi_N(r_{N,1})\right)+i_L\left(0,\psi_N(r_{N,2})\right)\right)} f_{N,N}\left(r_{N,1}, r_{N,2}\right), \end{aligned} \tag{50}$$

and

$$\hat{f}_{L,N}\left(r_{L,1}, r_{N,2}; R_\lambda\right) = e^{-2R_\lambda^{-2}\left(i_N\left(0,\psi_L(r_{L,1})\right)+i_L\left(0,\psi_N(r_{N,2})\right)\right)} f_{L,N}\left(r_{L,1}, r_{N,2}\right), \tag{51}$$

$$\hat{f}_{N,L}\left(r_{N,1}, r_{L,2}; R_\lambda\right)$$

$$= e^{-2R_\lambda^{-2}\left(i_L\left(0,\psi_N(r_{N,1})\right)+\, i_N\left(0,\psi_L(r_{L,2})\right)\right)} f_{N,L}(r_{N,1}, r_{L,2}; R_\lambda), \tag{52}$$

where $0 < r_{L,1} < r_{L,2}$ in (49), $0 < r_{N,1} < r_{N,2}$ in (50), $0 < r_{L,1}$ and $\psi_L(r_{L,1}) < r_{N,2}$ in (51). Finally, $0 < r_{N,1}$, $\psi_N(r_{N,1}) < r_{L,2}$ in (52).

Proof: The events in which a UE can connect to the two nearest LoS cells as its first and second choice happen when the path losses from the two nearest LoS are smaller than path losses from the two nearest NLoS stations. It is equivalent to the following conditional probability $\mathbb{P}(L_{L,L} | \boldsymbol{R_{L,1}} = r_{L,1}, \boldsymbol{R_{L,2}} = r_{L,2})$ defined in Section 4.3. As a result, the distribution is expressed as

$$\hat{f}_{L,L}(r_{L,1}, r_{L,2}; R_\lambda) = \mathbb{P}(L_{L,L} | \boldsymbol{R_{L,1}} = r_{L,1}, \boldsymbol{R_{L,2}} = r_{L,2}) f_{L,L}(r_{L,1}, r_{L,2}; R_\lambda).$$

Given the joint distribution of the distances from the serving stations to a typical user, we will derive the PDF of the distance of the second closest serving station in the subsequent section.

4.5 Distributions of the Distance to the Second Closest Serving Station

The PDF of the distance from the second closest serving base station to a typical user is introduced in the following corollary.

Corollary 2: The distribution of the distance from a typical user to its second nearest LoS station as a serving station is calculated as

$$\hat{g}_L(r_{L,2}; R_\lambda) = e^{-2R_\lambda^{-2} i_N\left(0,\psi_L(r_{L,2})\right)} g_L(r_{L,2}), \tag{53}$$

where $0 < r_{L,2}$ and $g_L(.)$ is the PDF of the distance from the second LoS cell to the typical user in (41). Similarly, the PDF of the distance from the second nearest NLoS station as a serving station of a typical user is evaluated as

$$\hat{g}_N(r_{N,2}; R_\lambda) = e^{-2R_\lambda^{-2}\, i_L\left(0,\psi_N(r_{N,2})\right)} g_N(r_{N,2}), \tag{54}$$

where $0 < r_{N,2}$ and $g_N(.)$ is the PDF of the distance from the second NLoS cell in (42).

Proof: The proof is omitted here as it follows the same approach in (11), in which there is one NLoS station within the ball that has the radius $\psi_L(r_{L,2})$. We now undergo steps to evaluate the SINR coverage probability of the second closest station and the two nearest stations in the following section.

4.6 SINR Coverage Analysis at the Second Station

Before computing the SINR coverage probability when users can connect to the two closest stations as their first and second options, we will introduce an essential theorem evaluating the SINR coverage probability when a mobile station connects to the second closest station based on Corollary 1 and Corollary 2.

Theorem 3: The SINR coverage probability at the second station $P_{C,2}(\gamma_2, R_\lambda)$ with the target threshold, γ_2 can be computed as

$$P_{C,2}(\gamma_2, R_\lambda) = P_{C,L,2}(\gamma_2, R_\lambda) + P_{C,N,2}(\gamma_2, R_\lambda), \tag{55}$$

where each term is the SINR coverage probability of the second closest LoS and NLoS base stations. Furthermore, each probability term can be evaluated as

$$P_{C,L,2}(\gamma_2, R_\lambda) = \int_0^\infty p_L(r_{L,2}; \gamma_2, R_\lambda)\hat{g}_L(r_{L,2}) dr_{L,2} \tag{56}$$

and

$$P_{C,N,2}(\gamma_2, R_\lambda) = \int_0^\infty p_N(r_{N,2}; \gamma_2, R_\lambda)\hat{g}_N(r_{N,2}) dr_{N,2}, \tag{57}$$

where $\hat{g}_L(.)$ and $\hat{g}_N(.)$ are distributions of the distances from a typical user to its serving stations, can either be NLoS or LoS, as a second choice. They are evaluated in (53) and (54). Meanwhile, $p_L(.)$ and $p_N(.)$ are defined in (16) and (17). The proof follows the same method in *Theorem 1*. Hence, it is omitted.

The joint SINR coverage probability of the two closest BSs will be presented in the next section.

4.7 SINR Coverage Probability Analysis using the Two Closest Stations

The following theorem provides a comprehensive approach assessing the SINR coverage probability when users associate with the two closest stations.

Theorem 4: The SINR coverage probability of the two closest stations $\bar{P}_{C,1/2}(\gamma_1, \gamma_2, R_\lambda)$ can be computed as

$$\bar{P}_{C,1/2}(\gamma_1, \gamma_2, R_\lambda) = 1 - \mathbb{P}(\boldsymbol{\gamma_{D,1}} < \gamma_1, \boldsymbol{\gamma_{D,2}} < \gamma_2; R_\lambda), \tag{58}$$

where $\boldsymbol{\gamma_{D,1}}, \boldsymbol{\gamma_{D,2}}$ are random variables representing the downlink SINR at the closest station and the second closest station, respectively. Moreover, $\mathbb{P}(\boldsymbol{\gamma_{D,1}} < \gamma_1, \boldsymbol{\gamma_{D,2}} < \gamma_2; R_\lambda)$ is the SINR outage probability, occurring when the SINRs from the two closest stations are below target thresholds. Hence, in this circumstance, a mobile station is considered not in the "coverage" areas of the nearest and the second nearest base stations. Since there are four independent scenarios in total, the SINR outage probability of each case is successively calculated as

$$\mathbb{P}(\boldsymbol{\gamma_{D,1}} < \gamma_1, \boldsymbol{\gamma_{D,2}} < \gamma_2; R_\lambda)$$
$$= \bar{P}_{L,L}(\gamma_1, \gamma_2, R_\lambda) + \bar{P}_{N,N}(\gamma_1, \gamma_2, R_\lambda) + \bar{P}_{L,N}(\gamma_1, \gamma_2, R_\lambda) + \bar{P}_{N,L}(\gamma_1, \gamma_2, R_\lambda). \tag{59}$$

We will evaluate each term in sequence as below. The first term in calculated as

$$\bar{P}_{L,L}(\gamma_1,\gamma_2,R_\lambda) = \iint_{r_{L,1}=0,r_{L,2}=r_{L,1}}^{\infty} \begin{matrix}\left(1-p_L(r_{L,1};\gamma_1,R_\lambda)\right)\left(1-p_L(r_{L,2};\gamma_2,R_\lambda)\right), \\ \times \hat{f}_{L,L}(r_{L,1},r_{L,2};R_\lambda)dr_{L,2}dr_{L,1}\end{matrix} \quad (60)$$

where $0 < r_{L,1} < r_{L,2}$, and $r_{L,1}$ is the distance from a typical user to the nearest LoS station, which UE associate as its first choice. Likewise, $r_{L,2}$ is the distances from the second closest LoS station as an alternative cell, and $p_L(.)$ are defined as the integrand of (16). Subsequently, for the second term, it can be evaluated as

$$\bar{P}_{N,N}(\gamma_1,\gamma_2,R_\lambda) = \iint_{r_{N,1}=0,r_{N,2}=r_{N,1}}^{\infty} \begin{matrix}\left(1-p_N(r_{N,1};\gamma_1,R_\lambda)\right)\left(1-p_N(r_{N,2};\gamma_2,R_\lambda)\right), \\ \times \hat{f}_{N,N}(r_{N,1},r_{N,2};R_\lambda)dr_{N,2}dr_{N,1}\end{matrix} \quad (61)$$

where $0 < r_{N,1} < r_{N,2}$ are distances from a typical user to the two nearest NLoS stations, respectively. Furthermore, $p_N(.)$ are defined as the integrand of (17). Subsequently, the SINR coverage probability for scenario C in Table 2 is given by

$$\bar{P}_{L,N}(\gamma_1,\gamma_2,R_\lambda) = \iint_{r_{L,1}=0,r_{N,2}=\psi_L(r_{L,1})}^{\infty} \begin{matrix}\left(1-p_L(r_{L,1};\gamma_1,R_\lambda)\right)\left(1-p_N(r_{N,2};\gamma_2,R_\lambda)\right), \\ \times \hat{f}_{L,N}(r_{L,1},r_{N,2};R_\lambda)dr_{N,2}dr_{L,1}\end{matrix} \quad (62)$$

where $r_{L,1} > 0$ and $r_{N,2} > \psi_L(r_{L,1})$ are the distances to the nearest LoS and the second nearest NLoS stations when a mobile station is associated with the nearest LoS and the second closest NLoS cell as its first and second serving BSs, and $\psi_L(.)$ is defined in (9). Finally, the last term in (59) is evaluated as

$$\bar{P}_{N,L}(\gamma_1,\gamma_2,R_\lambda) \quad (63)$$

$$= \iint_{r_{N,1}=0, r_{L,2}=\psi_N(r_{N,1})}^{\infty} \begin{matrix} \left(1 - p_N(r_{N,1}; \gamma_1, R_\lambda)\right)\left(1 - p_L(r_{L,2}; \gamma_2, R_\lambda)\right) \\ \times \hat{f}_{N,L}(r_{N,1}, r_{L,2}; R_\lambda) dr_{L,2} dr_{N,1} \end{matrix},$$

where $r_{N,1} > 0$ and $r_{L,2} > \psi_N(r_{N,1})$ are the distances from the first and second nearest LoS stations to a typical user in which the user considers the two closest LoS cells as its available options for serving base stations, and $\psi_N(.)$ is calculated in (12).

Proof: The joint SINR coverage probability is defined as the probability of the downlink SINRs from at least one of the two closest stations to an arbitrary UE exceeding a target threshold. Thus, the complementary of the joint SINR coverage probability is when the SINRs from the two nearest cells are below target thresholds. In other words, the joint SINR coverage probability can be expressed as

$$\bar{P}_{C,1/2}(\gamma_1, \gamma_2, R_\lambda) = 1 - \mathbb{P}(\boldsymbol{\gamma_{D,1}} < \gamma_1, \boldsymbol{\gamma_{D,2}} < \gamma_2; R_\lambda).$$

The complementary of the joint SINR coverage probability can be calculated by the sum of the probabilities of four mutually exclusive scenarios in Table 2 as follows

$$\mathbb{P}(\boldsymbol{\gamma_{D,1}} < \gamma_1, \boldsymbol{\gamma_{D,2}} < \gamma_2; R_\lambda)$$
$$= \bar{P}_{L,L}(\gamma_1, \gamma_2, R_\lambda) + \bar{P}_{N,N}(\gamma_1, \gamma_2, R_\lambda) + \bar{P}_{L,N}(\gamma_1, \gamma_2, R_\lambda) + \bar{P}_{N,L}(\gamma_1, \gamma_2, R_\lambda).$$

The evaluation for each probability term in the above equation can be achieved as follows

$$\bar{P}_{L,L}(\gamma_1, \gamma_2, R_\lambda)$$

$$\overset{(a)}{=} \iint_{r_{L,1}=0, r_{L,2}=r_{L,1}}^{\infty} \begin{matrix} \mathbb{P}(\boldsymbol{\gamma_{D,1}} < \gamma_1, \boldsymbol{\gamma_{D,2}} < \gamma_2; R_\lambda | C_L r_{L,1}^{-\alpha_L} > C_N r_{N,1}^{-\alpha_N}, C_L r_{L,2}^{-\alpha_L} > C_N r_{N,2}^{-\alpha_N}) \\ \times \hat{f}_{L,L}(r_{L,1}, r_{L,2}; R_\lambda) dr_{L,2} dr_{L,1} \end{matrix}$$

$$\overset{(b)}{=} \iint_{r_{L,1}=0, r_{L,2}=r_{L,1}}^{\infty} \begin{matrix} \mathbb{P}(\boldsymbol{\gamma_{D,1}} < \gamma_1; R_\lambda | C_L r_{L,1}^{-\alpha_L} > C_N r_{N,1}^{-\alpha_N}) \\ \times \mathbb{P}(\boldsymbol{\gamma_{D,2}} < \gamma_2; R_\lambda | C_L r_{L,2}^{-\alpha_L} > C_N r_{N,2}^{-\alpha_N}) \hat{f}_{L,L}(r_{L,1}, r_{L,2}; R_\lambda) dr_{L,2} dr_{L,1} \end{matrix}$$

$$\overset{(c)}{=} \iint_{r_{L,1}=0, r_{L,2}=r_{L,1}}^{\infty} \begin{matrix} \left(1-p_L(r_{L,1};\gamma_1,R_\lambda)\right)\left(1-p_L(r_{L,2};\gamma_2,R_\lambda)\right) \\ \times \hat{f}_{L,L}(r_{L,1},r_{L,2};R_\lambda)dr_{L,2}dr_{L,1} \end{matrix},$$

where (a) is the conditional probability for an event where a mobile station considers the first and second closest LoS stations as its serving stations, (b) follows the fact that the two stations are mutually exclusive in the sense that if one station is used, the other station will not be used. Therefore, given the distances from an arbitrary UE to the stations, the SINRs from the two stations are independent. Finally, (c) is derived in the same method as in Theorem 1. Similarly, the remaining terms can be calculated in the same manner.

We will derive the CCDF of the joint SINR outage probability of the two nearest stations in the following corollary.

Corollary 3: The joint CCDF of the downlink SINR outage probability of the first and the second nearest stations is calculated as

$$\begin{aligned} P_{C,1/2}(\gamma_1,\gamma_2,R_\lambda) = \mathbb{P}\left(\boldsymbol{\gamma_{D,1}} > \gamma_1, \boldsymbol{\gamma_{D,2}} > \gamma_2; R_\lambda\right) = P_{L,L}(\gamma_1,\gamma_2,R_\lambda) \; + \\ P_{N,N}(\gamma_1,\gamma_2,R_\lambda) + P_{L,N}(\gamma_1,\gamma_2,R_\lambda) + P_{N,L}(\gamma_1,\gamma_2,R_\lambda), \end{aligned} \tag{64}$$

where

$$P_{L,L}(\gamma_1,\gamma_2,R_\lambda) = \iint_{r_{L,1}=0, r_{L,2}=r_{L,1}}^{\infty} \begin{matrix} p_L(r_{L,1};\gamma_1,R_\lambda)\, p_L(r_{L,2};\gamma_2,R_\lambda) \\ \times \hat{f}_{L,L}(r_{L,1},r_{L,2};R_\lambda)dr_{L,2}dr_{L,1} \end{matrix}, \tag{65}$$

$$P_{N,N}(\gamma_1,\gamma_2,R_\lambda) = \iint_{r_{L,1}=0, r_{L,2}=r_{L,1}}^{\infty} \begin{matrix} p_N(r_{N,1};\gamma_1,R_\lambda)\, p_N(r_{N,2};\gamma_2,R_\lambda) \\ \times \hat{f}_{N,N}(r_{N,1},r_{N,2};R_\lambda)dr_{N,2}dr_{N,1} \end{matrix}, \tag{66}$$

$$P_{L,N}(\gamma_1,\gamma_2,R_\lambda)=\iint_{r_{L,1}=0,r_{N,2}=\psi_L(r_{L,1})}^{\infty} \begin{matrix} p_L(r_{L,1};\gamma_1,R_\lambda)\,p_N(r_{N,2};\gamma_2,R_\lambda) \\ \times\ \hat{f}_{L,N}(r_{L,1},r_{N,2};R_\lambda)dr_{N,2}dr_{L,1} \end{matrix}, \quad (67)$$

and

$$P_{N,L}(\gamma_1,\gamma_2,R_\lambda)=\iint_{r_{N,1}=0,r_{L,2}=\psi_N(r_{N,1})}^{\infty} \begin{matrix} p_N(r_{N,1};\gamma_1,R_\lambda)\,p_L(r_{L,2};\gamma_2,R_\lambda) \\ \times\ \hat{f}_{N,L}(r_{N,1},r_{L,2};R_\lambda)dr_{L,2}dr_{N,1} \end{matrix}, \quad (68)$$

Proof: The proof is similar to that of Theorem 4, hence, omitted.

In summary, the comprehensive analysis of the SINR coverage probability for the second closest station and the joint SINR coverage probability for the two closest base stations has been studied extensively in this chapter. More importantly, this approach can be abstracted to the wireless networks, which consider more than two stations. Analogously, the method to calculate the SINR coverage performance of mobile networks provides fundamental steps to incorporate essential factors residing at the physical layer to evaluate the average blocking probability when the URLLC users are rejected by the two nearest base stations.

Chapter 5: Blocking Probability Analysis of the Two Closest Base Stations

This chapter will estimate the average blocking probability of a particular user being rejected by their two nearest stations within the wireless network. Similar to the model at the first station, our model at the second cell will also incorporate several key techniques to support URLCC traffic. They include flexible frame structure, prioritized scheduling, pre-emption capability, resource provisioning for a URLLC packet. Moreover, time diversity by packet retransmission and spatial diversity of multiple base stations are also incorporated to enable URLLC. Additionally, by considering the average blocking probability experienced by users at two stations as a single entity, we can recursively evaluate the average blocking probability for cellular networks, which consider multiple BSs. As we want the second closest base station to provide the same QoS standard, the second BS is assumed to have identical physical and link models. First, the following section will investigate the distributions of all classes of users who seek services at the second closest BS due to being blocked at their nearest stations.

5.1 User Classes Distributions at the Second Nearest Base Station

Blocked users from their closest station are again divided into C classes based on their downlink SINRs at the second nearest base station. To keep the same QoS criterion at the second closest cell, the number of classes and boundaries for each SINR segment remains identical as in the closest station. The probability of a specific user being assigned into class c at the second station is defined as follows

$$\hat{P}_{C,2}(c; R_\lambda) = P_{C,2}(T_c, R_\lambda) - P_{C,2}(T_{c+1}, R_\lambda), \tag{69}$$

where $P_{C,2}(.)$ is computed in (55), representing the probability of the downlink SINR at a typical user at any time exceeding a certain SINR threshold. Similarly, class 0 users indicate the group of UEs that are rejected by their second closest cells. The probability for a mobile station identified as class i, j at the closest and the second closest station, respectively, is given by

$$\begin{aligned} \hat{P}_{1/2}(i, j; R_\lambda) &= \mathbb{P}\left(T_i \leq \boldsymbol{\gamma_{D,1}} < T_{i+1}, T_j \leq \boldsymbol{\gamma_{D,2}} < T_{j+1}; R_\lambda\right) \\ &= P_{C,1/2}\left(T_{i+1}, T_{j+1}, R_\lambda\right) - P_{C,1/2}\left(T_{i+1}, T_j, R_\lambda\right) - P_{C,1/2}\left(T_i, T_{j+1}, R_\lambda\right) + \\ &\quad P_{C,1/2}\left(T_i, T_j, R_\lambda\right), \end{aligned} \tag{70}$$

where $P_{C,1/2}(.)$ is computed in (64). The next section will derive the arrival rate of blocked users coming leaving their closest stations to join the second nearest cells.

5.2 Arrival Rate of Blocked Users at the Nearest Second Station

Figure 5-1 illustrates a process where mobile stations (marked as black asterisks) blocked by their closest base stations (marked as red points) seek alternative services at the second closest stations. A base station serves users who stay within its Voronoi tessellation with the highest priority because they consider the base station their closest cell. In case of an unstable physical link or insufficient resource, a UE rejected by the closest cell could try to initiate a new connection with the second closest cell. For instance, users who are rejected by *BS-3* and *BS-11* establish alternative connections with *BS-7*. Meanwhile, within *BS-2*'s Voronoi diagram, the cell accepts new connection requests from a mobile station blocked by its closest cell, *BS-5*.

In contrast, when a mobile station near the cell edge of *BS-2*'s Voronoi tessellation is blocked, it seeks alternative services by associating with *BS-4*, its second closest base station. Therefore, the number of blocked and new users joining a base station's Voronoi diagram fluctuates continuously. However, we assume the average number of users that

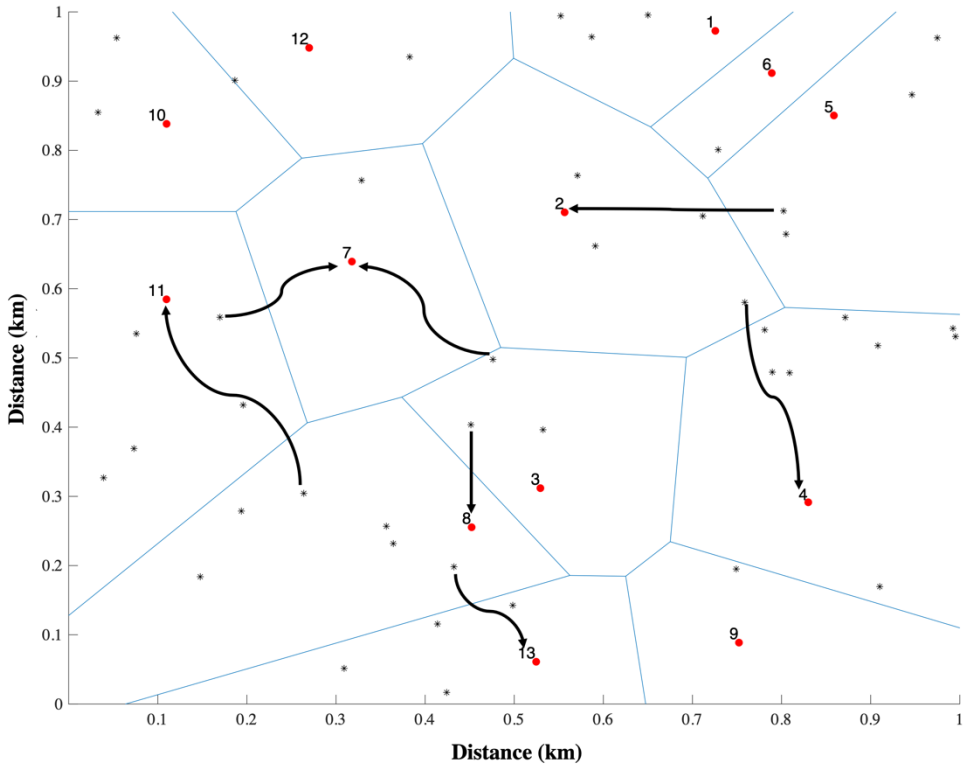

Figure 5-1 Illustration of situations in which mobile stations, that are rejected by their closest station terminate connection with the closest BS and join the second closest base station.

have been rejected by a cell equals the average number of users trying to access the second nearest station. It is typically the case when the system is in a steady state.

As a result, the distribution of class *c* users, being blocked by the nearest base stations, at the second closest cells follows a PPP distribution with an average rate

$$\bar{\lambda}_{2,c}(R_\lambda) = \bar{\lambda}\, P_{B,1}(R_\lambda)\hat{P}_2(c; R_\lambda), \tag{71}$$

where $\bar{\lambda}$ denotes the average number of users falling in the Voronoi diagram of each cell and $P_{B,1}(R_\lambda)$ indicates the average blocking probability that a particular UE experiences at the first cell. Additionally, $\hat{P}_{C,2}(c; R_\lambda)$ is calculated by (69) referring to the likelihood of the downlink SINR from the second closest BS within the c-th SINR segment. Next, to receive downlink URLLC packets, the required resource in the time-frequency plane at the second closest cell of blocked users, coming from their closest cells, will be evaluated under the finite block-length regime in the next section.

5.3 Resource Provisioning at the Second Nearest Station

Analogous to Section 3.3, our model incorporates finite blocklength mechanisms to determine resource allocations for URLLC packets. To transfer L information bits with the decoding error probability δ, the channel uses for class c users with downlink SINR $\gamma_{2,c}$ at the second nearest BS are approximately given by

$$\bar{r}_{2,c} \approx \frac{L}{n(\gamma_{2,c})} + \frac{(Q^{-1}(\delta))^2 \bar{n}(\gamma_{2,c})}{2(n(\gamma_{2,c}))^2} + \frac{(Q^{-1}(\delta))^2 \bar{n}(\gamma_{2,c})}{2(n(\gamma_{2,c}))^2} \sqrt{1 + \frac{4Ln(\gamma_{2,c})}{\bar{n}(\gamma_{2,c})(Q^{-1}(\delta))^2}}, \tag{72}$$

where $\gamma_{D,2,c}$ is the downlink SINR of class c users from the second closest station.

Presumably, a single shot URLLC packet of class c UE occupies a bandwidth of $f_{2,c}$ for a duration $t_{2,c}$. The relationship between required channel uses and the needed resource in the time-frequency plane is akin to that at the closest cell and is given by

$$f_{2,c} = \frac{\bar{r}_{1,c}}{\varepsilon t_{2,c}}, \tag{73}$$

where the constant ε is identical to that of the closest station if the same OFDMA frame structure and numerology are adopted at the second closest cell. We will consider the

resource constraint of the total available bandwidth at the second closest base station in the subsequent section.

5.4 Resource Provisioning Constraints at the Second Closest Base Stations

Class c users at the second closest BS will use a bandwidth of $f_{2,c}$ during their active periods b_A. Furthermore, the average active and idle periods of a typical user remain unchanged at the second closest station that are $B_A = E[b_A]$ and $B_I = E[b_I]$. Analogous to Section 3.4, the number of active users who access the second closest base stations is governed by the Poisson Process with the arrival rate or the average number of active class c users per millisecond is given by

$$\lambda_{2,c}(R_\lambda) = \frac{B_A}{B_A + B_I} \bar{\lambda}_{2,c}(R_\lambda) \tag{74}$$

Let $N_{2,c}(t)$ be the number of class c users at time t then $\lambda_{2,c} = E\left[N_{2,c}(t)\right]$. The average load of class c users in the second nearest cell is calculated as

$$\rho_{2,c}(R_\lambda) = \lambda_{2,c}(R_\lambda) B_A \tag{75}$$

We assume that users accessing their closest stations can pre-empt traffic from users associating stations, not as their closest stations. The probability of such pre-emptive events is analogous to the situation that users are blocked by their closest and second closest stations. The possibility of such an event to happen is controlled to be very small as the objective of this thesis. Consequently, the second closest BS serves mobile stations located within its Voronoi diagram and accommodates users blocked from their closest cells at the same time. Given the total available bandwidth W, the condition of a rejected UE from its closest station classified as a class c user at the second closest being blocked will be

$$f_{2,c} + \sum_{\tilde{c}=1}^{\mathcal{C}} f_{1,\tilde{c}} N_{1\tilde{c}}(t) + \sum_{\tilde{c}=1}^{\mathcal{C}} f_{2,\tilde{c}} N_{2,\tilde{c}}(t) > W, \quad (76)$$

where $f_{1,\tilde{c}}$ and $N_{1,\tilde{c}}(t)$ are the allocated bandwidth and the number of class $\tilde{c}$ users for whom the base station is the nearest. The blocking probability is always one for class 0 users whether they are blocked users coming from their closest cells or active users from whom the base station is the closest. The delay bound of URLLC packets class c users will be discussed in the next section.

5.5 Delay Bound under HARQ at the Second Nearest Station

Under the QoS requirements of URLLC communication, the upper bound of URLLC packet transmission time to class *c* users from their closest stations are discussed in Section 3.5. Suppose that the processing time, scheduling delay, and channel access are ignored. If the closest station cannot serve UE instantly, a mobile station will immediately switch to the second nearest cell. Then the allocated duration to transmit a single URLLC packet at the second closest station is tied by $\sum_{m=1}^{M_c} t_{2,c,m} + M_c D_{2,c} \leq D$, where $D_{2,c}$ is the feedback delay from UE to the second closest BS. Finally, we assume that the second closest station also assigns an identical interval for each transmission, $t_{2,c,m} = t_{2,c}$. Thus, the transmission interval for blocked mobile stations classified as class *c* users at the second closest cell is bounded as

$$t_{2,c} = \frac{D}{M_c} - D_{2,c} \quad (77)$$

Next, the following section will provide the analytical formula of the blocking probability at the second nearest station of users rejected by their closest station.

5.6 Blocking Probability at the Second Station

The following lemma presents the service interruption probability at the second base station under the assumption that users who access to the BS as their nearest are independent to those accessing the BS as the second nearest station.

Lemma 9: The blocking probability of blocked users, rejected by their closest stations, at the second nearest base stations is given by

$$P_{B,2}(c;R_\lambda)=\frac{\sum_{\boldsymbol{n_2}\epsilon \boldsymbol{S}_{2,c}}\prod_{\tilde{c}=1}^{\mathcal{C}}\left(\frac{\rho_{1,\tilde{c}}(R_\lambda)^{n_{1,\tilde{c}}}}{n_{1,\tilde{c}}!}\right)\prod_{\tilde{c}=1}^{\mathcal{C}}\left(\frac{\rho_{2,\tilde{c}}(R_\lambda)^{n_{2,\tilde{c}}}}{n_{2,\tilde{c}}!}\right)}{\sum_{\boldsymbol{n_2}\epsilon \boldsymbol{S_2}}\prod_{\tilde{c}=1}^{\mathcal{C}}\left(\frac{\rho_{1,\tilde{c}}(R_\lambda)^{n_{1,\tilde{c}}}}{n_{1,\tilde{c}}!}\right)\prod_{\tilde{c}=1}^{\mathcal{C}}\left(\frac{\rho_{2,\tilde{c}}(R_\lambda)^{n_{2,\tilde{c}}}}{n_{2,\tilde{c}}!}\right)},\tag{78}$$

where the vector $\boldsymbol{n_2}=\left(n_{1,1},n_{1,2},\dots,n_{1,\mathcal{C}},n_{2,1},n_{2,2},\dots,n_{2,\mathcal{C}}\right)$ denotes the number of users connecting to the cell as their first and second nearest stations. Additionally, $\boldsymbol{f_2}=\left(f_{1,1},f_{1,2},\dots,f_{1,\mathcal{C}},f_{2,1},f_{2,2},\dots,f_{2,\mathcal{C}}\right)$ is a vector denoting the allocated bandwidth for all users and, $\boldsymbol{S_2}=\{\boldsymbol{n_2}\mid \boldsymbol{f_2}\boldsymbol{n_2}^{\boldsymbol{T}}\le W\}$ consists all possible states that the station can accommodate all users' URLLC traffics. Finally, the vector consists of all blocking states of class c is defined as $\boldsymbol{S_{2,c}}=\{\boldsymbol{n_2}\mid \boldsymbol{n_2}\in \boldsymbol{S_2},\ \boldsymbol{n_2}+\boldsymbol{e_{2,c}}\notin \boldsymbol{S_2}\}$, where $\boldsymbol{e_{2,c}}$ is a unit vector with only the c^{th} entry for users accessing the base station as their second closest cell is non-zero element. In other words, $\boldsymbol{S_{2,c}}$ contains system states that the second closest BS cannot accommodate any additional incoming downlink URLLC packet destined to blocked users classified as class c at the second closest BS. The derivation of this lemma is analogous to *Lemma 5*.

The average blocking probability for a mobile station being blocked by the two nearest stations will be calculated in the next section.

5.7 Average Blocking Probability at the Two Nearest Stations

Suppose a user's closest station is A and the second closest station is B. Because the blocking probability for accessing the closest station is typically small, the number of UEs blocked by A and happened to join B at any time is minimal, so is the reverse case. Therefore, the event that a user being blocked by B given its SINR with respect to B can be treated as independent from the event that the user being blocked by A given its SINR with respect to A. With this assumption, a certain UE has the average probability of being blocked by both closest and second closest stations is computed in the following theorem.

Theorem 5: The probability that the two nearest stations block a typical URLLC user is computed as

$$P_{B,1/2}(R_\lambda) = \sum_{c_1=0}^{\mathcal{C}} \sum_{c_2=0}^{\mathcal{C}} P_{B,2}(c_2; R_\lambda) P_{B,1}(c_1; R_\lambda) \hat{P}_{1/2}(c_1, c_2; R_\lambda), \tag{79}$$

where c_1, c_2 are the class index at the first and second nearest stations, respectively, and $P_{B,1}(.)$, $P_{B,2}(.)$ are the blocking probabilities of a particular class UE defined in (35) and (78) at the first and second station in that order. Finally, $\hat{P}_{1/2}(c_1, c_2; R_\lambda)$ computed in (69) is the probability that a mobile station is classified as a member of a class c_1 and c_2 in the first and the second station, respectively.

Proof: following the total probability theorem, the average blocking probability of the two closest stations can be expressed as follows

$$P_{B,1/2}(R_\lambda) = \sum_{c_1=0}^{\mathcal{C}} \sum_{c_2=0}^{\mathcal{C}} \mathbb{P}\left(B_1, B_{2,} c_1, c_2; R_\lambda\right)$$

$$\overset{(a)}{=} \sum_{c_1=0}^{\mathcal{C}} \sum_{c_2=0}^{\mathcal{C}} \mathbb{P}(B_1, B_2 | c_1, c_2; R_\lambda) \hat{P}_{1/2}(c_1, c_2; R_\lambda)$$

$$\overset{(b)}{=} \sum_{c_1=0}^{\mathcal{C}} \sum_{c_2=0}^{\mathcal{C}} \mathbb{P}(B_2|B_1, c_1, c_2; R_\lambda)\mathbb{P}(B_1|c_1, c_2; R_\lambda)\hat{P}_{1/2}(c_1, c_2; R_\lambda)$$

$$\overset{(c)}{=} \sum_{c_1=0}^{\mathcal{C}} \sum_{c_2=0}^{\mathcal{C}} \mathbb{P}(B_2|B_1, c_2; R_\lambda)\mathbb{P}(B_1|c_1; R_\lambda)\hat{P}_{1/2}(c_1, c_2; R_\lambda)$$

$$\overset{(d)}{=} \sum_{c_1=0}^{\mathcal{C}} \sum_{c_2=0}^{\mathcal{C}} P_{B,2}(c_2; R_\lambda)P_{B,1}(c_1; R_\lambda)\hat{P}_{1/2}(c_1, c_2; R_\lambda)\,,$$

where B_1, B_2 are the blocking events occurring at the nearest and the second nearest cells, respectively, (a) and (b) are derived from Bayes' theorem. Moreover, (c) follows the pattern in which the blocking probability at the first station B_1 varies between classes and is independent of the classification of users at the second cell, as shown in (35). Finally, (d) is obtained based on the fact that B_2 depends merely on B_1 and c_2 as shown in (70) and (78).

In summary, this chapter has provided an approach to evaluate the blocking probability at the second nearest cell and calculates the average probability that both stations reject to deliver URLLC traffic to a mobile station. Furthermore, analytical expressions of the blocking probability at the second cell and the average blocking probability of the two nearest cells are derived. Subsequently, numerical results are illustrated in the next chapter.

Chapter 6: Numerical Results

This chapter will illustrate the numerical results of the SINR coverage probability at the closest station first. Numerical outcomes of the blocking probability at the closest station are presented subsequently. Finally, this chapter will conclude with the performance in terms of SINR coverage probability and blocking probability of wireless networks supporting URLLC traffics when considering the second closest base stations. Moreover, Table 3 summarizes all the parameters used throughout this chapter. In this chapter, we used parameters tailored to mmWave systems supporting URLLC traffic. They are values used in other papers, such as [19], [21], and [36]. The mmWave bands are chosen as an example to illustrate our proposed methods.

6.1 Analytical Result of the Performance URLLC System at the Closest Station

The mmWave network is operated at the frequency, $V = 28$ GHz, and the total available bandwidth assigned to each user is $W = 50$ MHz. The path loss exponents for LoS and NLoS links are $\alpha_L = 2$ and $\alpha_N = 4$, respectively, and the path loss intercepts are calculated as $C_L = C_N = (V/4\pi)^2$. The parameters for Nakagami fading are $N_L = 3$ and $N_N = 2$. The LoS function is defined as $b(r) = e^{-\beta r}$, where $\beta = 1/141.4\ m^{-1}$. The antenna pattern at base stations is fixed at $(M_T, S_T, \theta_T) = (20\ dB, 0\ dB, 30^o)$. For users, the beam pattern is fixed at $(M_R, S_R, \theta_R) = (10\ dB, -10\ dB, 45^o)$.

We assume the information bits $L = 1000$ bits for URLLC services. The latency requirement $D = 1$ msec and the system is required to maintain 99.9999% reliability or the packet error rate $\Delta = 10^{-6}$. Users are classified into 11 classes in total, from class 0 to

class 10 based on their downlink SINR at the first and the second stations. The maximum latency for acknowledgment packets from UE to the base station is $D_c = 0.125$ msec, $\forall c = 1, \ldots, 10$. A base station allows up to $M_c = 5, \forall c = 1, \ldots, 10$ re-transmission attempts for a single URLLC packets. The decoding error probability, δ, is chosen to fulfill the reliability requirement represented by $\delta^{M_c} \leq \Delta$. The arrival rate of active users for each cell is $\bar{\lambda} = 10$ users/msec, and the average active and idle periods are $B_A = B_I = 1$ msec, respectively. Additionally, the SINR thresholds used in section are -3 dB and 0 dB which are typical values. The signal power equals to noise power at 0 dB and at -3 dB, the signal power equals to half of the noise power. Especially, for -3 dB, the half-power point is a commonly used definition for the cut-off frequency in signal processing.

The association probabilities at the closest BS with different average cell radii are demonstrated in Figure 6-1. It shows that the likelihood that a typical user is associated with a LoS station increases as the cell radius shrinks. This is because a smaller cell radius indicates that the inter-site distance between base stations becomes smaller, in other words, the densification of base stations grows higher. Additionally, the smaller the distance from the nearest station to a particular user, the more likely the serving link is not blocked by any obstacles. Moreover, Figure 6-1 indicates that in a sufficiently dense network ($R_\lambda <$ 100 meters), the downlink signal at UE is determined mainly by the distribution of LoS base stations.

The SINR coverage probability as a function of cell radii and SINR thresholds are visualized in Figure 6-2. The numerical results shows that the mmWave networks typically require a small cell radius to achieve sufficient SINR coverage, and the SINR coverage

Table 3 Parameters for numerical results

Parameters	**Value**
V	28 GHz
W	50 MHz
β	$1/141.4\ m^{-1}$
P_t	30 dBm
σ^2	$(-174$ dBm/Hz $+10\ log_{10}(W)$ + noise figure of 10 dB) / P_t
(α_L, α_N)	$(2, 4)$
$C_L = C_N$	$\left(\frac{V}{4\pi}\right)^2$
(N_L, N_N)	$(3, 2)$
(M_T, S_T, θ_T)	$(20\ dB, 0\ dB, 30^o)$
(M_R, S_R, θ_R)	$(10\ dB, -10\ dB, 45^o)$
L	1000 bits
Δ	10^{-6}
D	1 msec
D_c	0.125 msec
M_c	5
$\bar{\lambda}$	10 users/msec
B_A	1 msec
B_I	1 msec

probability for a first station is considerably sensitive to the base station density. Additionally, further densifying the network does not improve the distributions of SINR since while a typical user receives higher serving power corresponding to the numerator of SINR's equation in (2), the interference term in the denominator of SINR's equation rises as well.

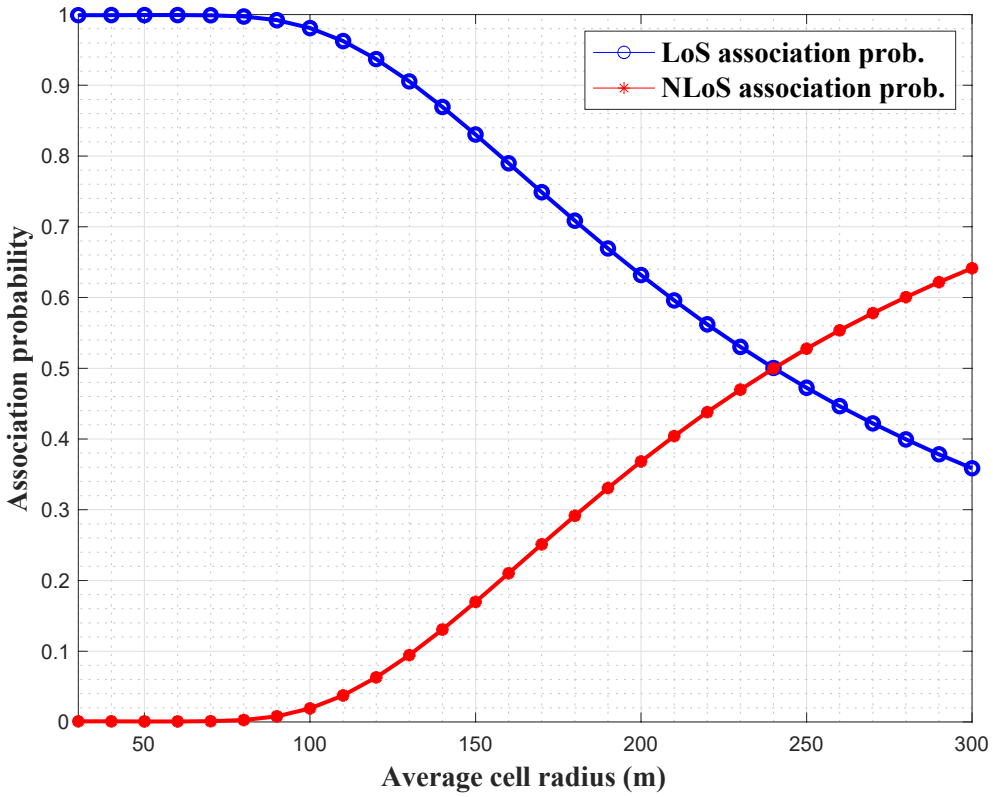

Figure 6-1 The association probability in (9) and (10) of a typical user to the serving LoS/NLoS base stations with various cell sizes.

The non-monotonic trend of the distribution of SINR coverage probability with base station density suggests a phase transition between the domination of noise and interference terms in the denominator of (2). When the density is low, decreasing the cell

sizes is equivalent to reducing the distance of the serving BS to a typical UE, e.g., from $R_\lambda = 100$ meters to $R_\lambda = 80$ meters. Hence, the probability of serving BSs being LoS BS increases, which provides higher serving power received by a typical user. However, the interference term is not affected significantly as the interferers are still far enough and are less likely to be LOS stations to the typical user.

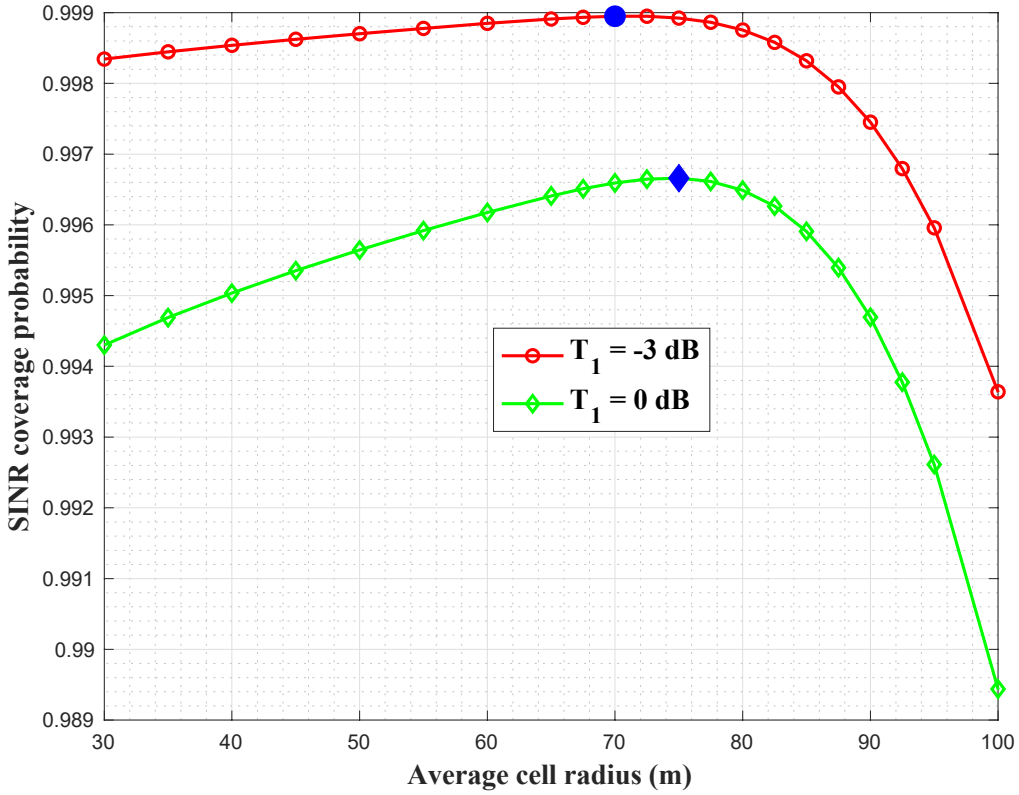

Figure 6-2 SINR Coverage Probability in (13) at various average cell radii, and different SINR thresholds.

The network eventually transits from noise-limited to interference-limited regime when there are enough interfering BSs after the network becomes sufficiently dense. When the base station density grows, there will be adequate strong LoS interferers, causing the SINR to degrade significantly. This point of views is illustrated by comparing the

distribution at $R_\lambda = 70$ meters and $R_\lambda = 30$ meters. Thus, there is an optimal density value highlighted in blue after which the performance of mmWave systems starts dropping. As shown in Figure 6-2, the optimal value of the network density depends on the SINR threshold γ_1. When $\gamma_1 = -3$ dB, the optimal value is around 70 meters, and the average cell size around 75 meters is the optimal size when $\gamma_1 = 0$ dB.

Figure 6-3 demonstrates the probability in which users of different classes are being blocked due to high traffic demand. We obtain the analytical results of the blocking probability for all classes with different SINR thresholds T_1. A base station will always reject mobile stations whose downlink SINRs are smaller than -3 dB or 0 dB. We consider

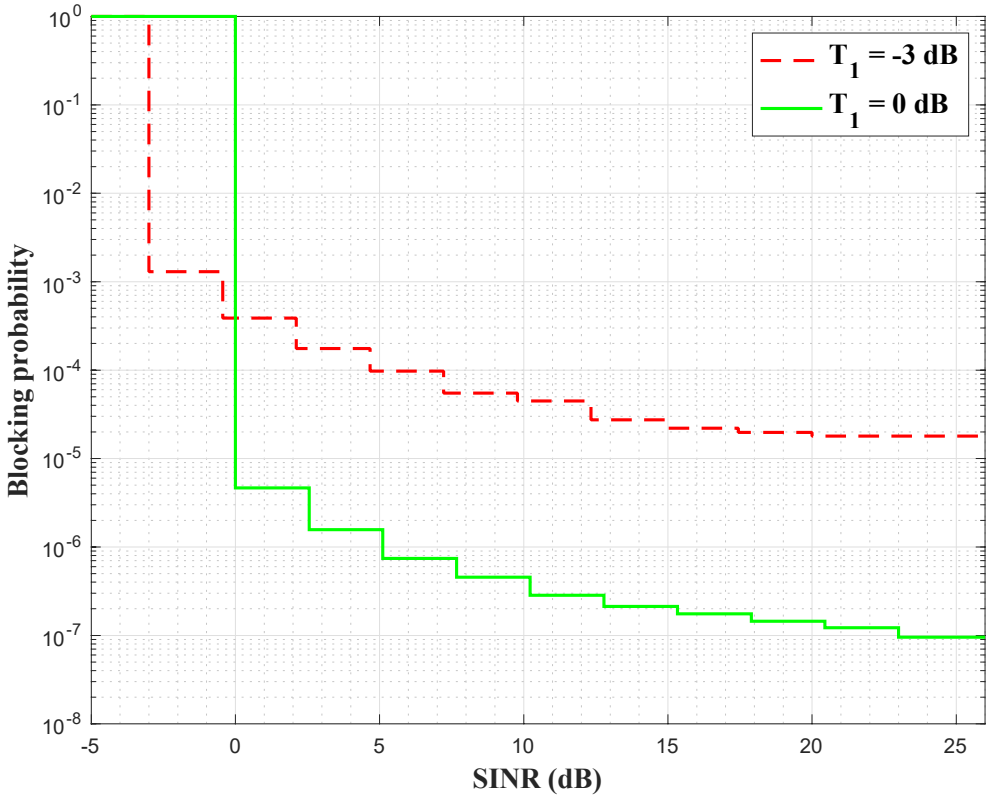

Figure 6-3 Blocking probability in (35) of each class at the closest station with $\boldsymbol{R_\lambda = 100}$ m and different SINR thresholds.

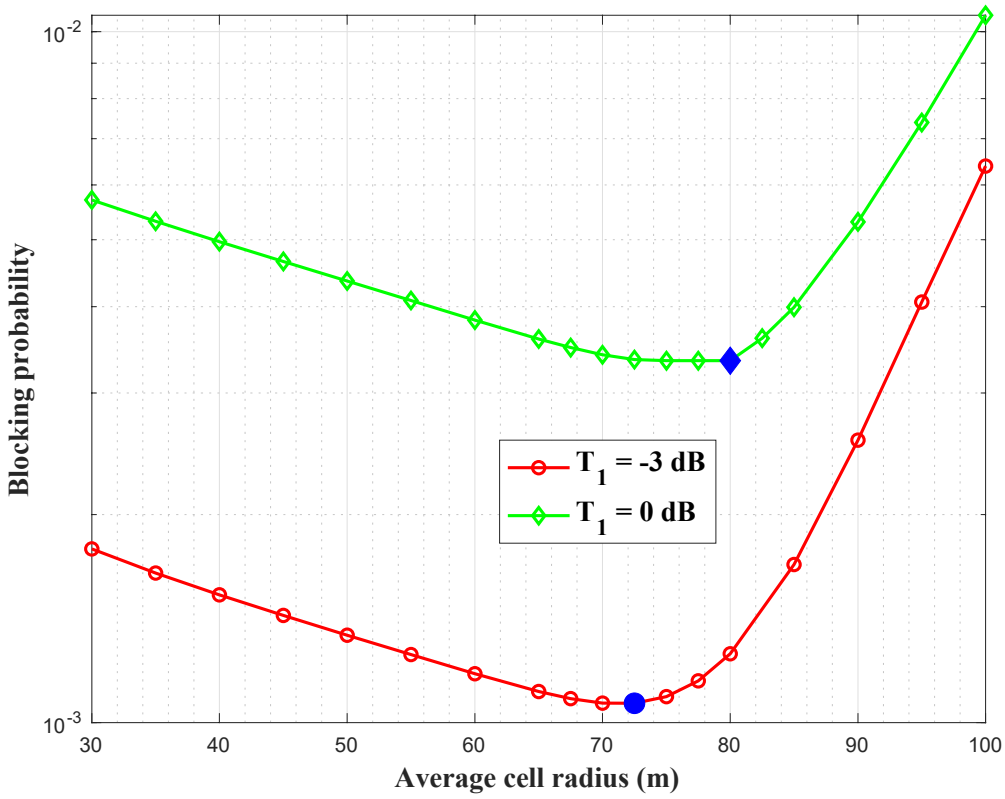

Figure 6-4 The average blocking probability experienced by a certain user at the closest station in (36) corresponding to different cell radii where $\boldsymbol{T_1 = \gamma_1}$.

them as class 0 users. Between all admitted classes, class 1 users require a considerable portion of the channel uses to deliver a URLLC packet. As a result, a base station needs to allocate the largest amount of bandwidth (to meet reliability requirements) for class 1 users; thus, they will be blocked most. In contrast, class 10 with the strongest downlink SINR are the group that is blocked least by their serving stations. In addition, when increasing SINR threshold T_1, class 0 becomes larger, more users will be blocked as class 0. This leaves fewer users for other classes, resulting in less resource usage and less blocking probability.

Subsequently, the effect of the average cell radius R_λ on the average blocking probability at the closest station is illustrated in Figure 6-4. The average blocking probability has a transition that follows the same general trend of the SINR coverage probability, as per Figure 6-2. However, at $T_1 = -3$ dB and 0 dB, the optimal cell radii for the average blocking probability are around 72.5 and 80 meters (highlighted in blue), which does not concur with the SINR results. The disagreement clearly comes from the fact that

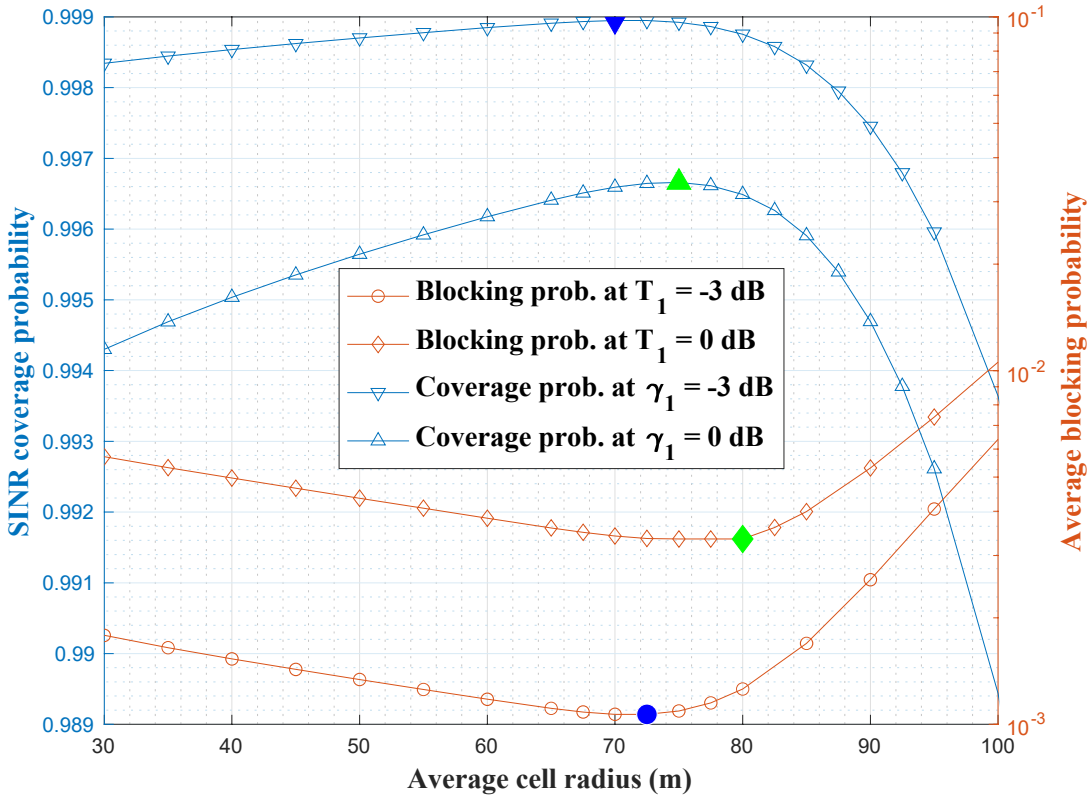

Figure 6-5 Comparison of the average blocking probability in (36) and the SINR coverage probability in (13) of the closest base station with $\boldsymbol{T_1}$ = −3 dB and $\boldsymbol{T_1}$ = 0 dB and $\boldsymbol{T_1 = \gamma_1}$, the SINR thresholds used to determine coverage probability equal the thresholds used to determine admissions for URLLC user classes.

SINR has different impacts on different user classes as demonstrated in Figure 6-4. Furthermore, the influence of physical parameters, SINR thresholds, and the densification of base stations on the average blocking probability and SINR coverage probability of the mmWave systems supporting URLLC services are summarized in Figure 6-5. The cell size that maximizes the coverage probability is not the same as the one that optimizes the average blocking probability due to the impacts of SINR thresholds and the physical models on the admitted user classes.

6.2 Analytical Result of the Performance URLLC System using Two Stations

To maintain the same QoS standard at the second closest BS, we use the same set of parameters of the closest station for the performance evaluation. First, we compare the association probability between four mutually exclusive scenarios in Table 2. As shown in Figure 6-6, the probability in which a typical user connects with a LoS station as one of its two nearest stations is exceptionally high in the dense network ($R_\lambda < 100$ meters). This can be comprehended because when the cell sizes are small, the probability that the serving link is associated with the closest LoS BS is extremely high, illustrated in Figure 6-1. Moreover, the same principle applies to the second closest station: which means when the densification of the BSs grows, a typical user is most likely associated with the second closest LoS station deployed in the near vicinity of the closest one. On the other hand, when the density of the cellular network becomes sparse, there is a greater possibility that blockages intercept links from a UE to two nearest stations. Therefore, the possibility of a typical user associated with the two closest NLoS base stations is quite large when the cell size of the cellular network increases.

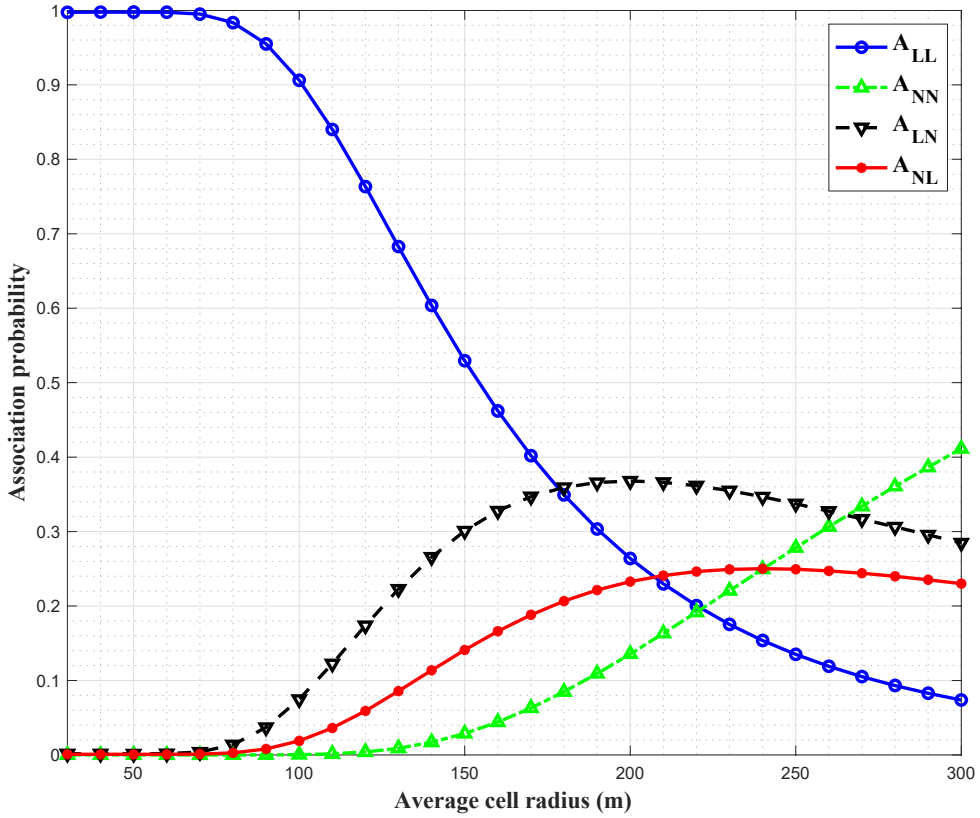

Figure 6-6 Association probability of the closest and second closest base stations in Section 4.3 with various average cell radii in four mutual exclusive scenarios in Table 2.

We assume the same SINR target threshold is employed at the second nearest cells to maintain the identical QoS standard between base stations. Figure 6-7 shows the improvement of the coverage SINR probability when considering the second closest BS with various target SINR thresholds as -3 dB and 0 dB. Compared with the performance at the closest station, the joint SINR coverage probability of the two nearest BSs enhances significantly. It could achieve an acceptable coverage ($> 99.8\%$) even when the cell radius is considerably large (≈ 100 meters) on average. When the downlink SINR from the closest station is smaller than a required SINR threshold due to high interference, or deep fading,

the mobile station may stay within the second closest cell located coverage area, thanks to the dense deployment of mmWave systems. Therefore, the average fraction of mobile users who achieve the desired SINR threshold at any time rises. As a result, the joint SINR coverage probability increases.

Additionally, the characteristic of the SINR coverage curve using two stations resembles the analogous non-monotonic trend of the coverage curve at the closest station. At a certain threshold of base station density when the network is sufficiently dense, mmWave networks switch from noise-limited to interference-limited behavior. Increasing the base station density does not improve the coverage of the mmWave cellular network since the likelihood of being interfered with by another strong LoS interference link at the two nearest BSs grows simultaneously.

The optimal values for SINR coverage probability are highlighted in Figure 6-7. The results show that the optimal cell size maximizing the joint SINR coverage probability depends on the target SINR threshold. Interestingly, compared to the closest station, the optimal cell radii for the joint SINR coverage probability are around $R_\lambda = 75$ and $R_\lambda = 80$ meters when $\gamma_1 = \gamma_2 = -3$ dB and $\gamma_1 = \gamma_2 = 0$ dB, respectively. However, those values do not agree with the SINR results at the closest station. The disagreement comes from the fact that in the sufficiently dense network ($R_\lambda < 100$ meters), the likelihood of a mobile station associating with the nearest LoS BS as its first choice and the second closest NLoS as its second option is substantial, as illustrated in Figure 6-6. In contrast, the probability of a user associated with the nearest NLoS station is negligible at the closest station, as shown in Figure 6-1.

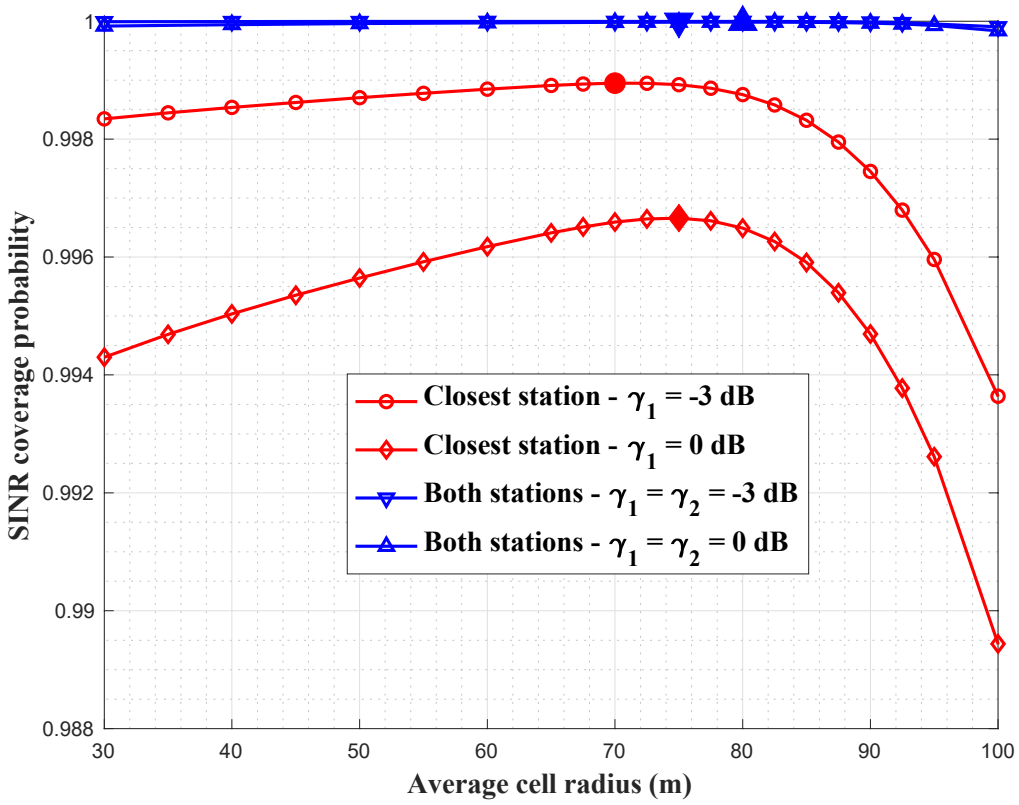

Figure 6-7 A comparison of SINR coverage probability performance in (58) between a single station and the scenario where UE rejected by its closest station can connect to the second closest BS at several cell radii and SINR thresholds.

The analytical results of the blocking probability at the second closest BSs for user classes are illustrated in Figure 6-8 with $R_\lambda = 100$ meters. Class 0 includes users whose downlink SINRs are below -3 dB. Compared with results at the closest serving stations, blocked UEs joining their second closest stations have a greater chance of being rejected at the second closest stations. The second nearest base station with identical resources not only accommodates high demand traffics required by users for whom the base station is the nearest but mobile stations rejected by their closest BSs due to unstable physical links or unavailability of resources to transmit URLLC packets immediately.

Subsequently, the numerical results of the average blocking probability experienced by a UE blocked by the two nearest BSs with different average cell radii are shown in Figure 6-9. By leveraging the minor cell size nature of mmWave cellular network to exploit the possibility of using the second nearest cell, the possibility in which the two nearest stations reject a mobile station falls considerably. The average probability

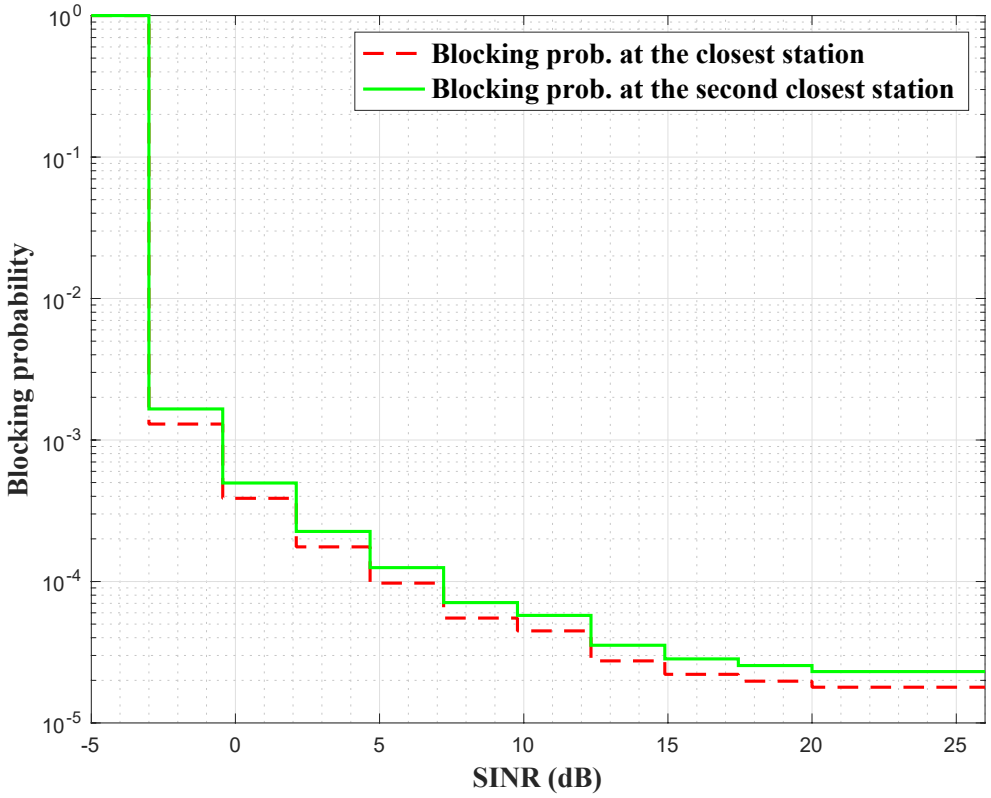

Figure 6-8 Comparison of Blocking Probability experienced by users at the closest station in (35) and at the second closest BSs in (78) with $\boldsymbol{R_\lambda = 100}$ m and $\boldsymbol{T_1 = -3}$ dB.

of a mobile station blocked by its two nearest stations is an order of magnitude smaller than the average blocking probability of the closest station when $T_1 = -3$ dB. Additionally, the blocking probability curve of both stations is a non-monotonic function of the average cell

radii following the same trend as in the closest stations. Moreover, the optimal cell radii (highlighted in Figure 6-9) minimizing the average blocking probability of the two nearest BSs experienced by UEs grow larger than the optimal cell sizes at the first stations. At $T_1 = -3$ dB and 0 dB, the optimal cell radii for the average blocking probability of both stations are around 77.5 and 82.5 meters, respectively which grow larger than the results at the closest station, around 72.5 and 80 meters at $T_1 = -3$ dB and 0 dB. The discrepancy is caused by the differences in distributions of user classes and the blocking probabilities of user classes at the second closest station, as shown in Figure 6-7 and Figure 6-8.

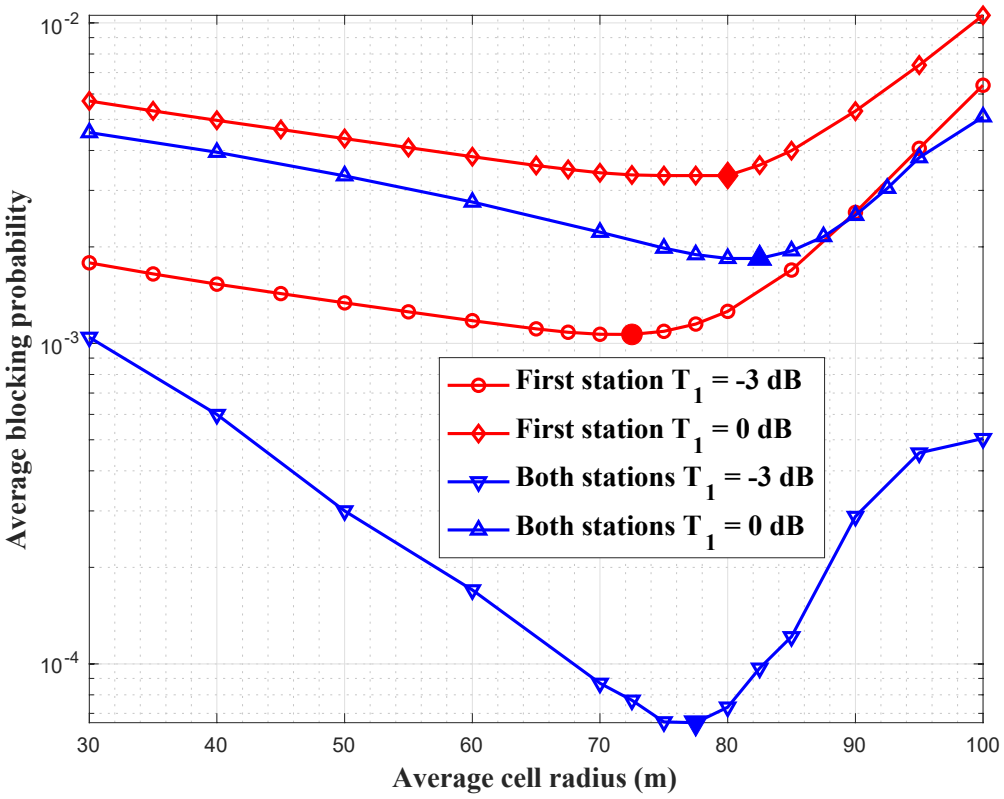

Figure 6-9 Comparison of blocking probability of a certain user at the closest base station in (36) and at two closest stations in (79) with different cell sizes, and $\boldsymbol{T_1} = -3$ dB.

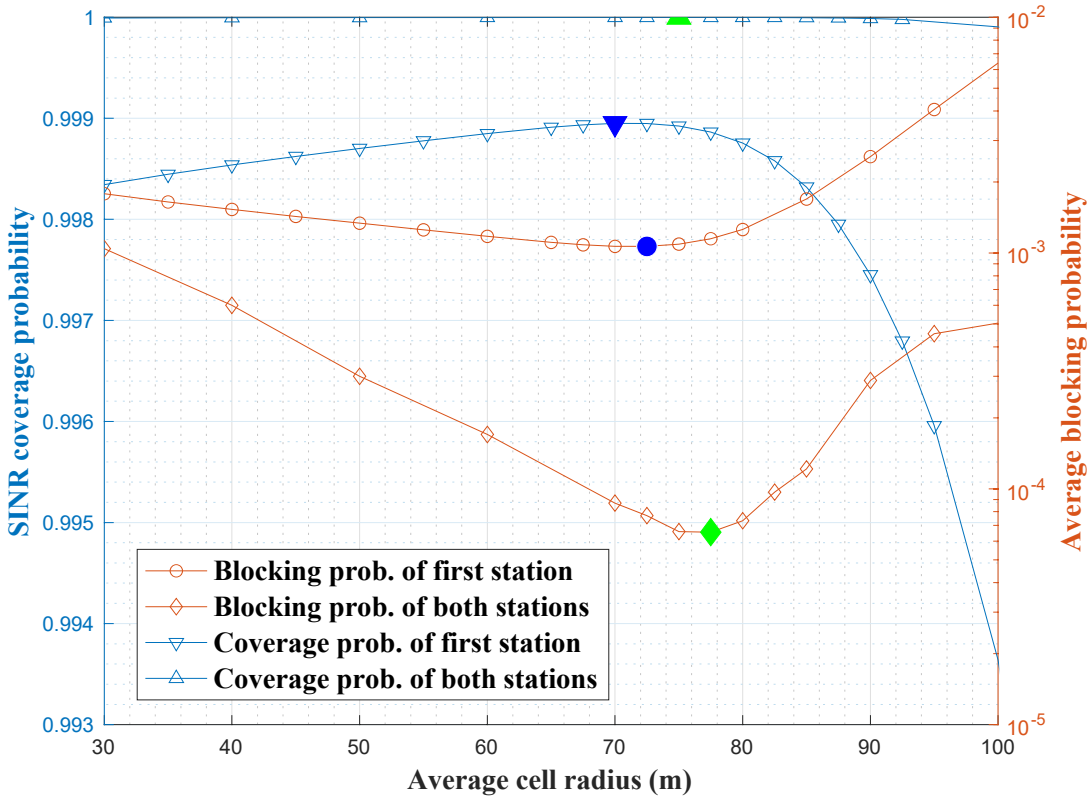

Figure 6-10 Numerical results comparison of SINR coverage probability and the average blocking probability performance for the closest station and the two closest stations at different cell sizes and $\boldsymbol{T_1 = \gamma_1 = \gamma_2 = -3}$ dB. For first station, SINR coverage and the average blocking probabilities are evaluated in (13) and (36). When considering the two nearest station, SINR coverage and the average blocking probabilities are evaluated in (58) and (79).

As a result, the spatial diversity of multiple stations helps mitigate the blocking probability experienced by a particular mobile terminal; thus, it alleviates the reliability requirements of URLLC communications while incorporating the HARQ re-transmission scheme and guaranteeing the total delay bound. Finally, the benefits of using the second nearest base stations in terms of SINR coverage probability and blocking probability at

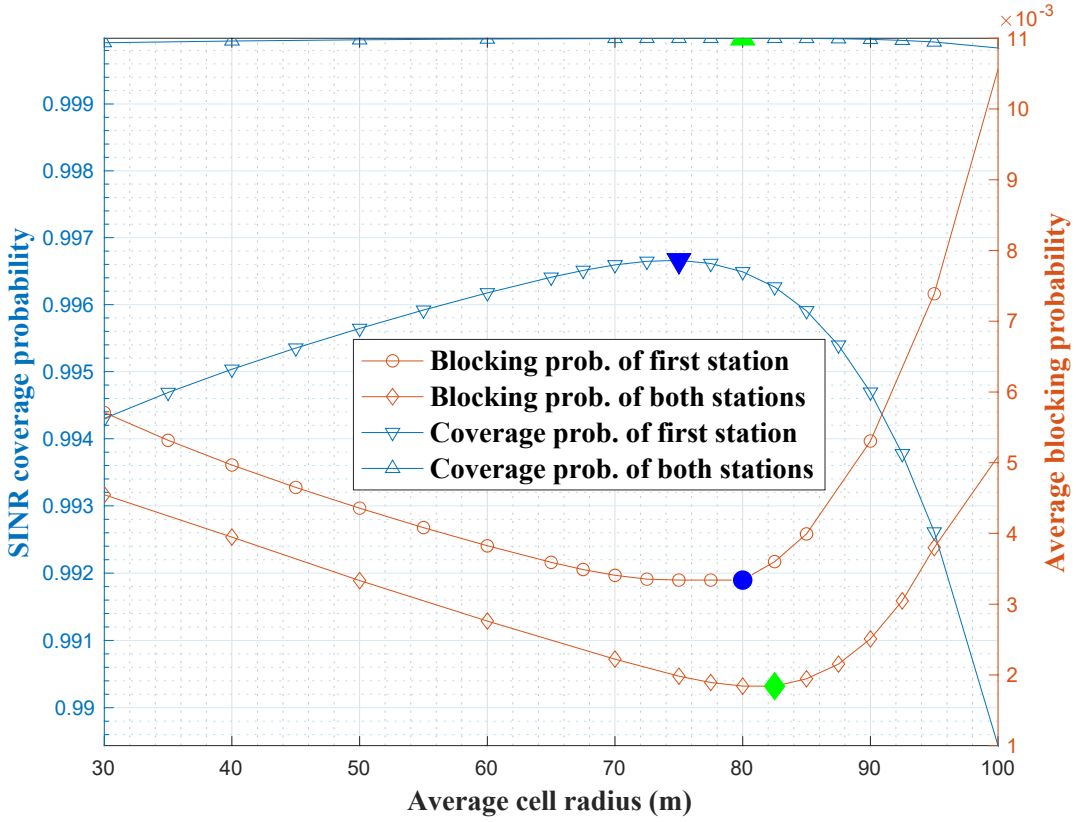

Figure 6-11 Numerical results comparison of SINR coverage probability and blocking probability performance for the closest station and the two closest stations at different cell sizes and $\boldsymbol{T_1 = \gamma_1 = \gamma_2 = 0}$ dB. For first station, SINR coverage and the average blocking probabilities are evaluated in (13) and (36). When considering the two nearest station, SINR coverage and the average blocking probabilities are evaluated in (58) and (79).

different SINR thresholds are illustrated in Figure 6-10 and Figure 6-11. The average blocking probability has a transition that follows the same general tendency of the SINR coverage probability either when considering the closest stations or the two closest stations. Additionally, the impacts of the parameters at the physical layer over the average blocking probability of the two closest BSs while explicitly considering the effects of delay, re-transmissions, and decoding failures remain. However, unlike the results derived at the

closest stations, when a second closest cell is used, the difference between values of the average cell radius to optimize the coverage area and the blocking probability does not grow larger when the SINR thresholds change from -3 dB to 0 dB. Moreover, with the same SINR thresholds, the optimal cell sizes for the SINR coverage and average blocking probabilities rise when the second closest cell is involved compared to their counterparts at the closest station.

Table 4 Summary of optimal cell radii for SINR coverage probability and average blocking probability

$T_1 = \gamma_1 = \gamma_2 = -3$ dB		
	SINR coverage probability	Average blocking probability
The closest station	70 m	72.5 m
The two closest stations	75 m	77.5 m
$T_1 = \gamma_1 = \gamma_2 = 0$ dB		
	SINR coverage probability	Average blocking probability
The closest station	75 m	80 m
The two closest stations	80 m	82.5 m

Therefore, numerical results derived in this chapter support the proposed method that utilizing the second closest base stations could be beneficial for network operators to plan or design an efficient cellular network supporting URLLC services. Furthermore, the proposed method provides an acceptable coverage probability even with the large cell radius and offers more flexible options for selecting/designing suitable transmission modes or coding schemes. Additionally, simply depending on the results of SINR coverage

probability for deploying wireless systems supporting URLLC services may not be enough since optimal values of the average cell radius optimizing the average blocking probability and SINR coverage probability do not concur (summarized in Table 4) either at the closet station or using the two nearest cells. Thus, ignoring the effect of the parameters residing at the physical layers while focusing merely on the data link factors or vice versa could result in an incorrect evaluation of the wireless network supporting URLLC services.

Although we do not run the Monte-Carlo simulation, our proposed approach has been analyzed mathematically. We derived and proved all equations. We will mainly use the same equations and assumptions when running simulations for the first station. For example, the SINR equation in (2) and all equations relating to allocated resources at the data link layer such as (29), (30), and (33) are used during simulations. Therefore, the difference between simulation and analytical results in one station case will be negligible. The only difference is that the simulation results will be for each user. In contrast, analytical results are based on statistical property, leading to the same results when the number of users is large based on the large number theorem.

We also use the same assumptions and equations for SINR and allocated resources at the data link layer when considering the second base station. However, the difference can be caused by different priority schemes when running simulations. We assumed that secondary users at the second station would have a lower priority than users who consider the BS as their first station for tractability. If the simulation uses the same scheme, then both the numerical and simulation results will have the same result. If the simulation chooses different scheme, the difference between simulation and analytical results in one station case will be negligible based on the work-preserving principle, the mean value does

not change with different scheduling algorithms, which means if one class is higher, the other class will be lower. Therefore, the blocking probability for first station users will be lower while the second station users will be higher than simulation results. Nevertheless, the overall average blocking probability will be the same.

The following chapter will conclude this dissertation with a well-constructed conclusion and discussions about potential future studies that can be explored based on this research.

Chapter 7: Conclusions and Future Work

In the last chapter, we will begin to discuss conclusions deduced from the results of previous chapters in this thesis and possible future research paths that motivated by this dissertation.

7.1 Key Conclusions

We have presented an in-depth study on estimating the average blocking probability for designing and deploying a next-generation wireless network, which incorporates enabling mechanisms at physical and link layers to support URLLC traffic. Key mechanisms to enable URLLC used in our models include diversity-based and structure-based techniques such as time diversity and flexible frame structure for URLLC packets at physical layers. At the same time, pre-emption capability and prioritized scheduling schemes of URLLC services are adopted at link layers. Finally, HARQ and spatial diversity of multiple BSs are also incorporated as cross-layer techniques to support URLLC.

We have shown that considering the secondary base stations improves performance. Therefore, the results could be used as another criterion to decide the trade-off between the cost and the performance for deploying next-generation cellular networks. The approach evaluating the mobile networks' performance when considering the second cell could be generalized similarly for the systems utilizing more than two base stations. Our model can help provide a performance guarantee for supporting URLLC services. Network carriers can use our model to plan their network deployment and decide suitable base station densities. They can also improve their networks by tuning various physical

and link layers factors based on their impacts on the performance as predicted by our models.

7.2 Future Work

Apart from proposing the novel approach to evaluate the performance of mmWave systems supporting URLLC traffic, this paper also paves the way for further explorations as follows:

1) Our analytical approach can be further extended by adopting different channel models statistically inferred by empirical data measured in urban cities [19]. Therefore, numerical results of the performance of wireless systems supporting URLLC traffic at those cities could be obtained beforehand and could provide insightful evaluation to plan network deployment.
2) Additionally, the performance of heterogeneous wireless systems could be one interesting future work for this thesis. For instance, in 5G network, it is more likely that mmWave base stations will be used to off-load high-speed or latency-sensitive data traffic for LTE networks. Therefore, studying the performance of URLLC services in this case is more practical.
3) Lastly, our proposed approach provides a method to evaluate the wireless link's performance as a first hop of the data path of a request from a mobile station to a data center and vice versa. Therefore, the impact of parameters of wireless links on the performance of different routing or scheduling algorithms on the overall network performance can be studied.

Bibliography

[1] P. Popovski, "Ultra-reliable communication in 5G wireless systems," *in Proceeding of 1st International Conference on 5G Ubiquitous Connectivity (5GU)*, pp. 146–151, Levi, Nov. 2014.

[2] M. Bennis et al., "Ultra-reliable and Low-latency Wireless Communication: Tail, risk and scale," *Proceedings of the IEEE*, vol. 106, no. 10, pp. 1834-1853, Oct. 2018.

[3] B. Holfeld, D. Wieruch, T. Wirth, L. Thiele, S. A. Ashraf, J. Huschke, I. Aktas, and J. Ansari, "Wireless communication for factory automation: an opportunity for LTE and 5G systems," *IEEE Communications Magazine*, vol. 54, no. 6, pp. 36–43, June 2016.

[4] O. N. C. Yilmaz, Y. P. E. Wang, N. A. Johansson, N. Brahmi, S. A. Ashraf, and J. Sachs, "Analysis of ultra-reliable and low-latency 5G communication for a factory automation use case," *in 2015 IEEE International Conference on Communication Workshop (ICCW)*, pp. 1190–1195, London, June 2015.

[5] M. Gidlund, T. Lennvall, and J. Akerberg, "Will 5G become yet another wireless technology for industrial automation?", *in IEEE International Conference on Industrial Technology (ICIT)*, pp. 1319–1324, Toronto, March 2017.

[6] K. I. Pedersen, G. Berardinelli, F. Frederiksen, P. Mogensen, and A. Szufarska, "A flexible 5G frame structure design for frequency-division duplex cases," *IEEE Communications Magazine*, vol. 54, no. 3, pp. 53–59, March 2016.

[7] Chairman's notes 3GPP: 3GPP TSG RAN WG1 Meeting 88bis, Available at https://www.3gpp.org/ftp/TSG_RAN/WG1_RL1/TSGR1_88b/Report, April 2017.

[8] 3GPP TSG RAN WG1 95, Tech. Rep., November 2018.

[9] P. Popovski, J. J. Nielsen, C. Stefanovic, E. de Carvalho, E. G. Str¨om, K. F. Trillingsgaard, A. Bana, D. Kim, R. Kotaba, J. Park, and R. B. Sørensen, "Ultra-reliable low-latency communication (URLLC): principles and building blocks," *CoRR, vol. abs/1708.07862*, 2017. [Online]. Available: http://arxiv.org/abs/1708.07862.

[10] G. Gashema, S. Bhardwaj, A. Abdukhakimov, D. S. Kim and J. M. Lee, "Spatial diversity to support URLLC through unlicensed spectrum in industrial wireless network systems", *in IEEE 3rd International Conference on Communication and Information Systems (ICCIS)*, pp. 141-145, Singapore, December 2018.

[11] G. J. Sutton, J. Zeng, R. P. Liu et al., "Enabling technologies for ultra- reliable and low latency communications: From PHY and MAC layer perspectives," *IEEE Communications Surveys and Tutorials*, vol. 21, no. 3, pp. 2488– 2524, 2019.

[12] H. Ji, S. Park, J. Yeo, Y. Kim, J. Lee, and B. Shim, "Ultra-reliable and low-latency communications in 5G downlink: Physical layer aspects," *IEEE Wireless Communications*, vol. 25, no. 3, pp. 124–130, Jun. 2018.

[13] B. Singh, Z. Li, O. Tirkkonen, M. A. Uusitalo, and P. Mogensen, "Ultra-reliable communication in a factory environment for 5G wireless networks: Link level and deployment study," *in IEEE Annual International Symposium on Personal, Indoor, and Mobile Radio Communications (PIMRC)*, pp. 1–5, Valencia, Sept 2016.

[14] S. Ashraf, Y. P. E. Wang, S. Eldessoki, B. Holfeld, D. Parruca, M. Serror, and J. Gross, "From radio design to system evaluations for ultra-reliable and low-latency communication," *in Proceedings of European Wireless Conference*, pp. 1–8, Dresden, May 2017.

[15] 3GPP TR 38.912, "Study on New Radio (NR) access technology," v:15.0.0, Jul. 2018.

[16] Y. Polyanskiy, H. V. Poor, and S. Verdu, “Channel coding rate in the finite blocklength regime,” *IEEE Transactions on Information Theory*, vol. 56, no. 5, pp. 2307–2359, May 2010.

[17] 3GPP. 2017, “Downlink Multiplexing of eMBB and URLLC Transmission.” *3GPPTSG RAN WG1 NR Ad-Hoc Meeting*, R1-1700374, January 2017.

[18] 3GPP. 2016. *3GPP TSG RAN WG1 Meeting 87*, November 2016.

[19] C. P. Li, J. Jiang, W. Chen, T. Ji, and J. Smee, “5G ultra-reliable and low-latency systems design,” *in 2017 European Conference on Networks and Communications (EuCNC)*, pp. 1–5, Oulu, June 2017.

[20] A. Anand, G. de Veciana, and S. Shakkottai, “Joint Scheduling of URLLC and eMBB Traffic in 5G Wireless Networks,” Dec. 2017. [Online]. Available: https://arxiv.org/abs/1712.05344.

[21] L. You, Q. Liao, N. Pappas, and D. Yuan, “Resource Optimization with Flexible Numerology and Frame Structure for Heterogeneous Services,” *ArXiv e-prints*, Jan. 2018.

[22] T. S. Rappaport, R. W. Heath Jr., R. C. Daniels, and J. N. Murdock*, Millimeter Wave Wireless Communication*. Prentice Hall, 2014.

[23] Z. Pi and F. Khan, “An introduction to millimeter-wave mobile broad-band systems,” *IEEE Communication Magazine*, vol. 49, no. 6, pp. 101 –107, Jun. 2011.

[24] T. Rappaport et al., “Millimeter wave mobile communications for 5G cellular: It will work!” *IEEE Access*, vol. 1, pp. 335–349, 2013.

[25] G. Yang, M. Xiao, M. Alam, and Y. Huang, “Low-latency heterogeneous networks with millimeter-wave communications,” *IEEE Communication Magazine*, vol. 56, no. 6, pp. 124–129, June 2018.

[26] F. Boccardi et al., “Five Disruptive Technology Directions for 5G,” *IEEE Communication Magazine*, vol. 52, no. 2, pp. 74–80, Feb. 2014.

[27] T. Rappaport et al., “Broadband millimeter-wave propagation measurements and models using adaptive-beam antennas for outdoor urban cellular communications,” *IEEE Transactions on Antennas and Propagation*, vol. 61, no. 4, pp. 1850–1859, Apr. 2013.

[28] A. Alejos et al., “Measurement and analysis of propagation mechanisms at 40 GHz: Viability of site shielding forced by obstacles,” *IEEE Transactions on Vehicle Technology*, vol. 57, no. 6, pp. 3369–3380, 2008.

[29] S. Rajagopal, S. Abu-Surra, and M. Malmirchegini, “Channel feasibility for outdoor non-line-of-sight mmwave mobile communication,” *in Proceedings of IEEE Vehicle Technology Conference (VTC Fall)*, pp. 1–6, Quebec, 2012.

[30] M. Akdeniz, Y. Liu, M. Samimi, S. Sun, S. Rangan, T. Rappaport, and E. Erkip, “Millimeter wave channel modeling and cellular capacity evaluation,” *IEEE Journal on Selected Areas in Communications*, vol. 32, no. 6, pp. 1164–1179, June 2014.

[31] J. G. Andrews, F. Baccelli, and R. K. Ganti, “A tractable approach to coverage and rate in cellular networks,” *IEEE Transactions on Communications*, vol. 59, no. 11, pp. 3122–3134, Nov. 2011.

[32] H. S. Dhillon et al., “Modeling and analysis of K-tier downlink heterogeneous cellular networks,” *IEEE Journal on Selected Areas in Communications*, vol. 30, no. 3, pp. 550–560, April 2012.

[33] R. W. Heath Jr. et al., “Modeling heterogeneous network interference with using Poisson point processes,” *IEEE Transactions on Signal Processing*, vol. 61, no. 16, pp. 4114–4125, Aug. 2013.

[34] S. Akoum, E. O. Ayach, and R. W. Heath Jr., “Coverage and capacity in mmWave cellular systems,” *in Proceedings of Asilomar Conference*, pp. 688–692, Pacific Grove, Nov. 2012.

[35] T. Bai, R. Vaze, and R. Heath, “Analysis of blockage effects on urban cellular networks,” *IEEE Transactions on Wireless Communications*, vol. 13, no. 9, pp. 5070–5083, Sept. 2014.

[36] T. Bai and R. W. Heath Jr., “Coverage and rate analysis for millimeter wave cellular networks,” *IEEE Transactions on Wireless Communications*, vol. 14, no. 2, pp. 1100–1114, Oct. 2014.

[37] X. Yu, J. Zhang, M. Haenggi, and K. B. Letaief, “Coverage analysis for millimeter wave networks: The impact of directional antenna arrays,” *IEEE Journal on Selected Areas in Communications*, vol. 35, no. 7, pp. 1498–1512, Jul. 2017.

[38] X. Zhang and J. G. Andrews, “Downlink cellular network analysis with multi-slope path loss models”, *IEEE Transactions on Wireless Communications*, vol. 63, no. 5, pp. 1881-1894, May 2015.

[39] A. Anand and G. de Veciana, “Resource Allocation and HARQ Optimization for URLLC Traffic in 5G Wireless Networks,” *IEEE Journal on Selected Areas in Communications*, vol. 36, no. 11, pp. 2411–2421, Nov. 2018.

[40] A.K. Erlang, “Solution of some problems in the theory of probabilities of significance in automatic telephone exchanges,” *The Post Office Engineer’s Journal*, Vol. 10, pp. 189-197, 1917.

[41] H. Kobayashi, B. L. Mark, and W. Turin, Probability, Random Processes, and Statistical Analysis: Applications to Communications, Signal Processing, Queueing Theory and Mathematical Finance. *Cambridge University Press*, Feb. 2012.

[42] H. Kobayashi and B. L. Mark, “Generalized loss models and queueing-loss networks,” *International Transactions in Operational Research*, 9(1): pp. 97–112, 2002.

[43] A. Olutayo, J. Cheng, and J. F. Holzman, “A new statistical channel model for emerging wireless communication systems,” IEEE Open J. Commun. Soc. 1, 916 (2020).

[44] J. G. Andrews, T. Bai, M. N. Kulkarni, A. Alkhateeb, A. K. Gupta, R. W. Heath Jr., “Modeling and analyzing millimeter wave cellular systems,” *IEEE Transactions on Wireless Communications*, pp. 403–430, 2017

[45] F. Lemic, J. Martin et al., “Localization as a feature of mmWave communication,” *in International Wireless Communications and Mobile Computing Conference (IWCMC)*, pp. 1033–1038, Paphos, Sept 2016.

[46] M. A. Khan, N. Saeed, A. W. Ahmad, and C. Lee, ‘‘Location awareness in 5G networks using RSS measurements for public safety applications,’’ *IEEE Access,* vol. 5, p. 21753–21762, 2017.

[47] B. J. Silva and G. P. Hancke, “Non-line-of-sight identification without channel statistics,” *in IECON 2020 The 46th Annual Conference of the IEEE Industrial Electronics Society*, pp. 4489–4493, Singapore, 2020.

[48] Q. Zheng et al., “Channel non-line-of-sight identification based on convolutional neural networks,” *IEEE Wireless Communication Letters*, vol. 9, no. 9, pp. 1500–1504, Sep. 2020.